NATIONAL RENEWABLE ENERGY LABORATORY

An Energy Signal Tool for Decision Support in Building Energy Systems

Gregor P. Henze, Gregory S. Pavlak, Anthony R. Florita, Robert H. Dodier, and Adam I. Hirsch

NREL is a national laboratory of the U.S. Department of Energy
Office of Energy Efficiency & Renewable Energy
Operated by the Alliance for Sustainable Energy, LLC

This report is available at no cost from the National Renewable Energy Laboratory (NREL) at www.nrel.gov/publications.

Technical Report
NREL/TP-5500-63130
December 2014

Contract No. DE-AC36-08GO28308

An Energy Signal Tool for Decision Support in Building Energy Systems

Gregor P. Henze, Gregory S. Pavlak, Anthony R. Florita, Robert H. Dodier, and Adam I. Hirsch

Prepared under Task No. ARCB.1102

NREL is a national laboratory of the U.S. Department of Energy
Office of Energy Efficiency & Renewable Energy
Operated by the Alliance for Sustainable Energy, LLC

This report is available at no cost from the National Renewable Energy Laboratory (NREL) at www.nrel.gov/publications.

National Renewable Energy Laboratory
15013 Denver West Parkway
Golden, CO 80401
303-275-3000 • www.nrel.gov

Technical Report
NREL/TP-5500-63130
December 2014

Contract No. DE-AC36-08GO28308

This report is available at no cost from the National Renewable Energy Laboratory (NREL) at www.nrel.gov/publications.

Available electronically at http://www.osti.gov/scitech

Available for a processing fee to U.S. Department of Energy and its contractors, in paper, from:

U.S. Department of Energy
Office of Scientific and Technical Information
P.O. Box 62
Oak Ridge, TN 37831-0062
phone: 865.576.8401
fax: 865.576.5728
email: mailto:reports@adonis.osti.gov

Available for sale to the public, in paper, from:

U.S. Department of Commerce
National Technical Information Service
5285 Port Royal Road
Springfield, VA 22161
phone: 800.553.6847
fax: 703.605.6900
email: orders@ntis.fedworld.gov
online ordering: http://www.ntis.gov/help/ordermethods.aspx

Cover Photos: (left to right) photo by Pat Corkery, NREL 16416, photo from SunEdison, NREL 17423, photo by Pat Corkery, NREL 16560, photo by Dennis Schroeder, NREL 17613, photo by Dean Armstrong, NREL 17436, photo by Pat Corkery, NREL 17721.

NREL prints on paper that contains recycled content.

Executive Summary

This project demonstrates a prototype energy signal tool for operational whole-building and system-level energy use evaluation. The purpose of the tool is to provide a summary of building energy use that allows a building operator to quickly distinguish normal and abnormal energy use. Toward that end, energy use status is displayed as a traffic light, which is a visual metaphor for energy use that is either substantially different from expected (red and yellow lights) or approximately the same as expected (green light). Which light to display for a given energy end use is determined by comparing expected to actual energy use. As expected, energy use is necessarily uncertain; we cannot choose the appropriate light with certainty. Instead, the energy signal tool chooses the light by minimizing the expected cost of displaying the wrong light. The expected energy use is represented by a probability distribution. Energy use is modeled by a low-order lumped parameter model. Uncertainty in energy use is quantified by a Monte Carlo exploration of the influence of model parameters on energy use. Distributions over model parameters are updated over time via Bayes' theorem. The simulation study was devised to assess whole-building energy signal accuracy in the presence of uncertainty and faults at the submetered level, which may lead to tradeoffs at the whole-building level that are not detectable without submetering.

Table of Contents

List of Figures

List of Tables

Nomenclature

$\vec{a}$	action vector
a_{opt}	optimal action
$\mathbf{A}, \mathbf{B}, \mathbf{C}, \mathbf{D}$	state space model matrices
C	opaque building shell thermal capacitance
C_c	roof thermal capacitance
$C_{c,1}$	external node roof thermal capacitance
$C_{c,2}$	internal node roof thermal capacitance
C_e	exterior wall thermal capacitance
$C_{e,1}$	external node exterior wall thermal capacitance
$C_{e,2}$	internal node exterior wall thermal capacitance
C_f	floor thermal capacitance
$C_{f,1}$	external node floor thermal capacitance
$C_{f,2}$	internal node floor thermal capacitance
C_i	internal thermal capacitance
$C_{i,1}$	node 1 internal thermal capacitance
$C_{i,2}$	node 2 internal thermal capacitance
C_p	air thermal capacitance
C_z	zone thermal capacitance
CM	zone air capacitance multiplier
COP	coefficient of performance
D	measured data
DX	direct expansion
e_k	transfer function heat gain history coefficient
$E(x)$	expected value of x
E_{meas}	measured predicted energy consumption
E_{mod}	model-predicted energy consumption
$E_{0,low}$	lower threshold of low deviation
$E_{1,low}$	upper threshold of low deviation
$E_{0,high}$	lower threshold of high deviation
$E_{1,high}$	upper threshold of high deviation
EQP	equipment
G	central green light action
GM	internal gain multiplier
h_{fg}	heat of vaporization of water
HVAC	heating, ventilation, and air conditioning
i	action index
j	state index
K	cost matrix (decision analysis) or knowledge (inference)
LTG	lighting
m_{air}	mass of air in the zone

m	transfer function heat gain history order
M	model output
$\dot{m}_{inf}$	infiltration mass flow rate
$\dot{m}_{SA}$	supply air mass flow rate
ML	much lower state
MH	much higher state
NSU	nighttime setup
n	number of past inputs
$\vec{P}$	state probability vector
p	probability
$q_{occ,lat}$	occupant latent gains
$\dot{Q}_{ep}$	surrogate or measured sensible zone load
$\dot{Q}_{g,c}$	convective portion of internal gains (lighting, occupants, and equipment)
$\dot{Q}_{g,r,c}$	radiative fraction of internal gains applied to ceiling surface
$\dot{Q}_{g,r,e}$	radiative fraction of internal gains applied to vertical wall surface
$\dot{Q}_{g,r+sol,w}$	radiative portion of internal gains and solar radiation through glazing
$\dot{Q}_{inf}$	infiltration heat gain
$\dot{Q}_{sol,c}$	solar radiation transmitted through opaque ceiling/roof surfaces
$\dot{Q}_{sol,e}$	solar radiation transmitted through opaque vertical exterior surfaces
$\dot{Q}_{sol,w}$	solar radiation transmitted through glazing
$\dot{Q}_{sh}$	sensible convective heat gain to zone air
$\dot{Q}_{zs}$	sensible zone load
$\dot{Q}_{rom}$	reduced-order model predicted sensible zone load
r	number of elements in the input vector **u**
R_1	combined heat transfer coefficient to opaque shell mass node
R_2	conduction coefficient between mass and internal surface node
R_3	convection/radiation coefficient b/w surface and zone air temperature nodes
R_c	roof thermal resistance
$R_{c,1}$	roof combined external convection and radiation coefficient
$R_{c,2}$	roof conduction resistance
$R_{c,3}$	roof internal combined convection and radiation coefficient
R_e	exterior wall thermal resistance
$R_{e,1}$	combined external convection and radiation coefficient
$R_{e,2}$	exterior wall conduction resistance
$R_{e,3}$	exterior wall internal combined convection and radiation coefficient
R_f	floor thermal resistance
$R_{f,1}$	ground conduction coefficient
$R_{f,2}$	floor conduction resistance
$R_{f,3}$	floor internal combined convection and radiation coefficient
R_i	internal partition thermal resistance
$R_{i,1}$	internal partition combined convection and radiation coefficient
$R_{i,2}$	internal partition conduction resistance

$R_{i,3}$	internal partition combined convection and radiation coefficient
R_w	glazing thermal resistance
RA	return air
RH	upper red light action
RL	lower red light action
ROM	reduced-order model
RTU	rooftop unit
S	similar state
SA	supply air
SH	somewhat higher state
SHGC	solar heat gain coefficient
SL	somewhat lower state
$\mathbf{S}$	transfer function input coefficient matrix
t	time or time index
T_a	outdoor air temperature
T_c	ceiling node temperature
$T_{c,1}$	external roof node temperature
$T_{c,2}$	internal roof node temperature
T_e	exterior wall node temperature
$T_{e,1}$	external exterior wall node temperature
$T_{e,2}$	internal exterior wall node temperature
T_f	floor node temperature
$T_{f,1}$	external floor node temperature
$T_{f,2}$	internal floor node temperature
T_g	ground temperature
T_i	internal partition temperature
T_m	opaque building shell thermal temperature
T_s	(pseudo) internal surface temperature
T_z	zone air temperature
$\bar{T}_z$	average zone air temperature over timestep
$\mathbf{u}$	input variable vector
WBE	whole building electricity consumption
W_z	zone air humidity ratio
W_{OA}	outdoor air air humidity ratio
W_{SA}	supply air humidity ratio
$\mathbf{x}$	state variable vector
$\dot{\mathbf{x}}$	state variable first derivative vector
X_{high}	definition of high level of deviation threshold
X_{low}	definition of low level of deviation threshold
$\mathbf{y}$	output variable vector
YH	upper yellow light action
YL	lower yellow light action
σ_ε	measurement noise
$\Delta\tau$	time step

1 Introduction and Motivation

Stakeholders of assorted interests are increasingly concerned with the energy performance of the built environment. Increasing commitment to energy efficiency, cost-minimal retrofits, and renewable energy integration has coincided with the availability of commercial and open-source building energy simulation engines. Model-based approaches have become the norm, with engineering design accelerating its reliance on software. It is hypothesized that, beyond building design applications, model-based engineering of buildings can be extended to encompass a building's multi-decade life cycle. Of particular interest is the operational energy performance, where tradeoffs in comfort and energy consumption can be hidden, and the establishment of "normal behavior," as distinguished from "faulted behavior," is nontrivial. Research interests lie in data-driven models for decision-making processes that are flexible, adaptable, and can evolve with the engineered system.

A balance must be struck between model sophistication and available data. One may have scores of utility bill data available but little understanding of an appropriate, physically relevant model. Or one might have an exceedingly detailed physical model available but its real-world validity is still questionable because calibration has been performed against sparse utility data. Pattern recognition or classification can be used to ascertain the validity of a model and the value of data; however, building applications are in their infancy. At the building systems level, monitoring-based heating, ventilation, and air conditioning (HVAC) commissioning (Wang et al., 2013) and chiller fault detection (Zhao et al., 2013) have shown promise.

The interpretation of patterns might be further aided by providing real-time, appliance-level power management and occupant feedback for sociotechnical energy conservation (Gulbinas et al., 2014). At the whole-building level, participation in the smart grid via approaches such as energy storage may entail value-cognizant electricity demand shifting and shaping (Florita et al., 2013); the value to the building owner is likely different than that to the electricity grid. Data mining and knowledge discovery tasks have the ultimate goal of predictive diagnostics for buildings and their systems, and have shown acceptable levels of misclassification in the face of the evolving, nonstationary behavior common to buildings (Kiluk, 2014). Sector-wide studies include modeling the evolution and refurbishment of the German heating market (for 2050 goals) and its impact on carbon emissions (Bauermann et al., 2014).

The goal of the energy signal tool research is to enable owners and operators of commercial buildings to quickly (in a matter of seconds) attain insight into how their buildings' energy use compares against the likely range of expected energy consumption over a given time period (days, weeks, months, or years). The output of the energy signal tool is a simple traffic light indicator that summarizes energy consumption relative to model-based expectations. To find the appropriate value of the indicator, the energy signal tool carries out an analysis of building energy use, taking uncertainty and misclassification costs into account. As illustrated in Figure 1, the energy signal tool process begins with an operational energy model of a building to provide expected energy performance, but recognizes that any model only approximates reality.

Previous research explored how gray-box models are obtained and calibrated from noisy data (Pavlak et al., 2014), and results are extended here to include HVAC systems. The term operational derives from the desire to consider only a few influential variables within the model and to use them in real-time applications while learning from data as they are gathered. We believe that simplified operational models are sufficient when coupled to uncertainty analysis and misclassification costs of relatively simple building types such as big box retail. Work is currently underway to develop an open-source tool based on the OpenStudio development effort that would allow the decision analysis to be applied to arbitrarily complex multi-zone buildings.

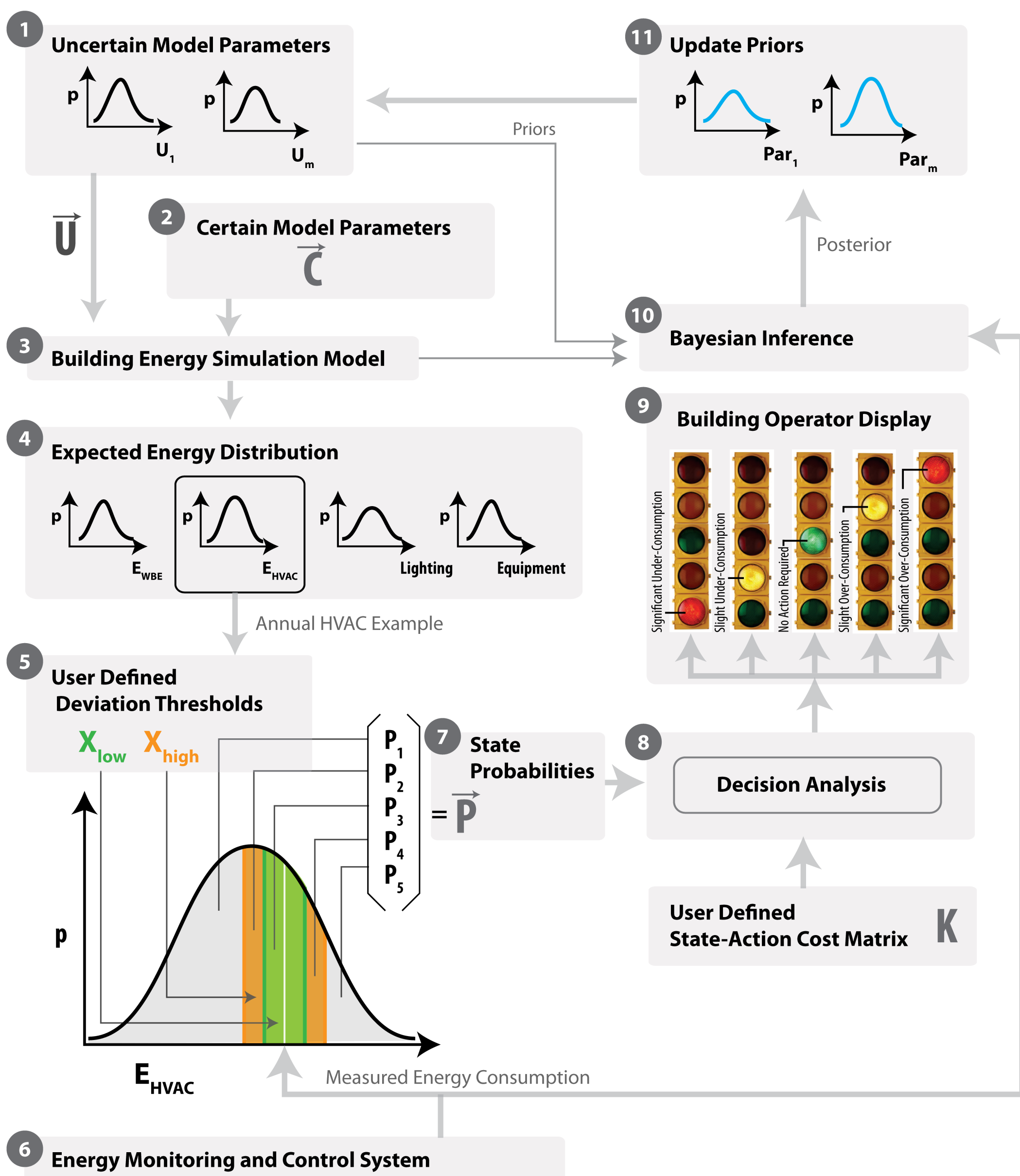

Figure 1. Energy signal tool flowchart

A Bayesian probabilistic approach was adopted here to update beliefs about uncertainties in light of new data. Over time, the energy signal tool learns improved assumptions for input parameter uncertainties by incorporating measured building data into a Bayesian inference process. Unobserved variables are inferred from data and physical modeling. The range of all possible values is divided into five exhaustive and mutually exclusive intervals, labeled 1–5 in the figure, which represent predicted energy use that is substantially lower, somewhat lower, more or less the same, somewhat higher, and substantially higher than observed. The probability that energy use (at either the whole-building or the end-use level) falls into a given range of values, is computed as the integral of the energy use probability distribution over that interval. User-defined thresholds determine the tool's sensitivity and are driven by the operator's risk appetite. We then applied utility theory to find the most appropriate action given an assumed cost of misclassification of each action (i.e., each traffic light color) in each state (i.e., each energy use interval probability). The expected cost of misclassification is the cost matrix multiplied by the probability vector. We chose the element of the expected cost that has the lowest value.

To illustrate the operation of the energy signal tool, we give examples of its output in various energy use scenarios and review Bayesian updates to model parameters.

2 Literature Review

Most uncertainties in building energy performance are addressed during the design phase. The evolution of a given design involves a sequence of decisions by various domain experts and has implications in thermal, visual, and acoustical performance (De Wit and Augenbroe, 2002). Competing objectives such as energy consumption, environmental performance, and financial costs warrant multi-objective optimization for decision-making (Diakaki et al., 2010, 2013). Although engineering tradeoffs lead to numerous optimal and near-optimal solutions; e.g., Pareto fronts (Rafiq, 2000), early design choices lead to the building's ultimate sustainability (Balcomb and Curtner, 2000). Confounding the problem is information sharing with conflicting objectives in the collaborative design process (Ugwu et al., 2000). However, the primary, uncertain drivers in the design process include (1) (micro)climate variables (Sun et al., 2014), which may not be appropriately captured by typical meteorological data; (2) occupancy patterns and dynamics, which may be hard to capture with traditional diversity factor approaches (Li et al., 2009); and (3) consideration for the existing infrastructure where the building will be constructed, which may be far from ideal (Takizawa et al., 2000). Judkoff et al. (2008/1983) described the sources of difference between simulation and reality. Recent interest lies in sustainable designs with renewable energy systems (Piotr et al., 2012), net zero energy buildings (Attia et al., 2012), and overall healthy and productive buildings (Choi et al., 2009; Zeiler et al., 2012).

Energy management or measurement and verification within existing building energy systems must face a plethora of uncertainties, including (but not limited to) noisy sensors, point measures of distributed phenomena (e.g., air temperature), and unobserved variables. To capture complex, nonlinear, and multivariable interactions, mathematical approaches such as Gaussian processes (Burkhart et al., 2014; Heo and Zavala, 2012), multi-agent decision-making control strategies (Zhao et al., 2010), and Bayesian-calibrated energy models (Heo et al., 2011; Neumann et al., 2011) have been used. Furthermore, with the proliferation of wireless sensor networks in smart buildings (De Farias et al., 2014), interest in assessing performance has extended beyond energy into mold growth and remediation (Moon and Augenbroe, 2008), as well as disaster preparedness and management (Filippoupolitis and Gelenbe, 2009; Vinh, 2009) for events such as fires (Sanctis et al., 2011), earthquakes (Basso et al., 2013), and bioterrorist attacks (Thompson and Bank, 2010). The literature shows that the need for decision support within operational building settings is vast, yet a balance between risk and situational usefulness needs to be attained.

Many authors have devised frameworks for decision support in various building energy performance settings. Augenbroe et al. (2009) described a tool with an investment strategy for energy performance decision-making for existing buildings with viable refurbishments via optimization. Kolokotsa et al. (2009) analyzed and categorized buildings for specific actions or groups of plans in a methodology for decision support of building energy efficiency and environmental quality, including real-time operation and offline decision-making. Das et al. (2010) considered building maintainability using an analytical hierarchy process to balance budget requirements with performance standards for nine building systems, including input from 37 facilities management experts. Gultekin et al. (2013) developed a decision support system for guidance in "green retrofits" to identify key criteria and feasible alternatives. Mohseni et al. (2013) offered a comprehensive decision-making methodology for condition monitoring to guide building asset managers, aiding capital investments and expenditures. In a series of papers, Lee et al. (2013a,b, 2012) detailed process models for decision support in energy-efficient building projects, and campus-scale infrastructures, and summarized a "workbench" for uncertainty quantification, respectively. Collectively, i.e., taking this series of three papers together, a decision support framework was provided.

3 Methodology

3.1 Modeling Environment

For prototyping the energy signal tool, the simulation study required the validation of the operational building energy model as detailed in the following sections. In practice, a measurement campaign combined with system identification techniques would be required before the energy signal tool is implemented. Because of its Bayesian learning approach, the process could be automated with a basic knowledge of the model's structure.

3.1.1 Retail Building Simulation Models

The U.S. Department of Energy's EnergyPlus standalone retail reference building (Crawley et al., 2001; Deru et al., 2010), post-1980 construction, was used as a relatively simple first application for prototyping and testing the energy signal tool. An isometric view of the original five-zone retail building is shown in Figure 2, along with a plan view of model zoning shown in Figure 3. One zone is dedicated to the entry vestibule, two slender zones to the left and right of the vestibule have glazing and are assumed to be affected by solar gains, a very large core retail zone occupies about 90% of the floor area. Finally, a loading and storage zone covers the back of the store. Selected model details are highlighted in Table 1. This five-zone EnergyPlus model was used to generate simulated operational data for use in developing the reduced-order building energy models described in the following subsections. Surrogate data were preferred here over real measurements so that latent variables could be controlled in the experimental study.

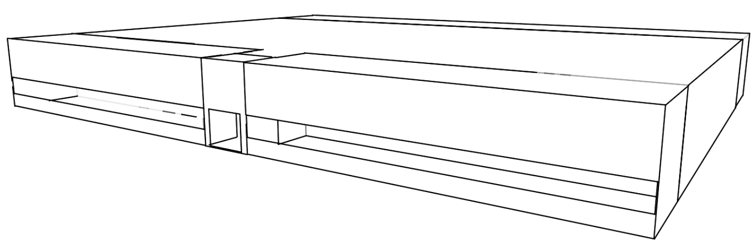

Figure 2. Isometric view of five-zone retail building model

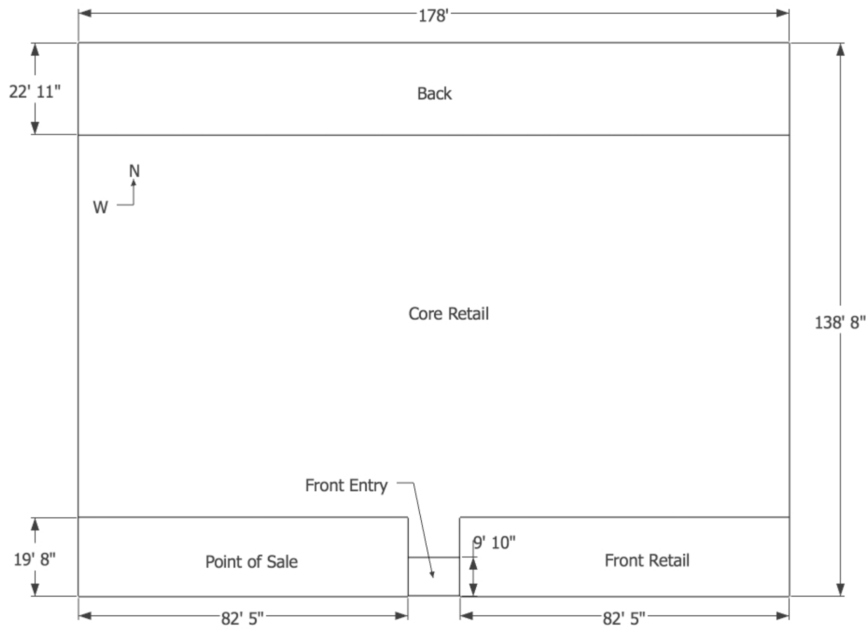

Figure 3. Zone plan of five-zone retail building model

Table 1. Selected EnergyPlus Model Details

Property	Value	Units
Vintage	1980	year
Volume	13 984	m^3
Conditioned floor area	2294	m^2
Bldg. avg. U-value (no film, excluding floor)	0.418	$W\,m^{-2}\,K^{-1}$
Ext. wall U-value (no film)	0.621	$W\,m^{-2}\,K^{-1}$
Roof U-value (no film)	0.314	$W\,m^{-2}\,K^{-1}$
Floor U-value (no film)	12.904	$W\,m^{-2}\,K^{-1}$
Internal thermal capacitance	450	$MJ\,K^{-1}$
Internal thermal capacitance per floor area	196.2	$kJ\,K^{-1}\,m^{-2}$
Infiltration	1.01	ACH
Glazing fraction	7	%
Glazing U-factor	3.354	$W\,m^{-2}\,K^{-1}$
Glazing solar heat gain coefficient	0.385	fraction
Lighting power density	32.3	$W\,m^{-2}$
Equipment power density	5.23	$W\,m^{-2}$
Occupant density	7.11	m^2/person
HVAC system	CV-DX	-

3.1.2 Inverse Gray-Box Building Model for Operational Applications

The inverse gray-box modeling approach developed for this work is largely based on methods described by Braun and Chaturvedi (Braun and Chaturvedi, 2002; Chaturvedi et al., 2000). For the application presented in this work, it is important to be able to predict transient cooling and heating requirements for the building using inverse models that are trained using on-site data. Inverse models for transient building loads range from purely empirical or "black-box" models to purely physical or "white-box" models. Generally, black-box (e.g., neural network) models require a significant amount of training data and may not always reflect the actual physical behavior, whereas white-box (e.g., finite difference) models require specification of many physical parameters. Braun and Chaturvedi introduced a hybrid or "gray-box" modeling approach that uses a transfer function with parameters that are constrained to satisfy a simple physical representation for energy flows in the building structure. A robust method was also presented for training parameters of the constrained model, wherein (1) initial values of bounds on physical parameters are estimated from a rough building description; (2) better estimates are obtained using a global direct search algorithm; and (3) optimal parameters are identified using a nonlinear regression algorithm. They found that 1 to 2 weeks of data are sufficient to train a model so that it can accurately predict transient cooling or heating requirements.

Previous to the work by (Braun and Chaturvedi, 2002; Chaturvedi et al., 2000), (Judkoff et al., 2000; Subbarao, 1988a,b; Subbarao et al., 1988, 1985), developed a modeling scheme consisting of several lumped parameters with direct correspondence to reality and correspondence to a detailed model. The model, used in combination with field data, enabled empirical determination of the input parameters, thereby reducing model uncertainty.

Inverse gray-box models may be based on the approximation of heat transfer mechanisms by an analogous electrical lumped resistance-capacitance network. This approximation creates a flexible structure that allows the modeler to choose the appropriate level of abstraction. Model complexity can range from representing entire systems with a few parameters to modeling each heat transfer surface with numerous parameters. Depending on the model structure and complexity, parameters can approximate the physical characteristics of the system. Model parameters are then identified through a training period with measured data.

Figure 4 shows the 21-parameter thermal network representations that by Braun and Chaturvedi (2002); Chaturvedi et al. (2000) found to work well. Other forms have been considered in this work and are described below. A separate 3R2C network is used to represent external wall, ceiling, ground, and internal wall heat transfer. Looking at the 3R2C network for exterior walls, for example, $R_{e,1}$ could be thought to represent a combined external convection and radiation coefficient, $R_{e,2}$ wall conduction resistance, and $R_{e,3}$ internal combined convection and radiation coefficient to the zone air node. Solar gains from opaque elements are represented by $\dot{Q}_{sol,e}$ applied to the external surface nodes (e.g., $T_{e,1}$ and $T_{c,1}$). Storage is neglected for glazing elements that are represented by a single resistance R_w. Solar gains directly entering the zone through glazing are distributed among internal partition nodes $T_{i,1}$ and $T_{i,2}$ as $\dot{Q}_{sol,w}$. Internal gains are split into convective and radiant fractions. Convective fractions are applied directly to the zone air node T_z as $\dot{Q}_{g,c}$. Radiant portions are applied to interior surface nodes $T_{e,2}$ and $T_{c,2}$ as $\dot{Q}_{g,r,e}$ and $\dot{Q}_{g,r,c}$, respectively. (Split is proportional by surface area.)

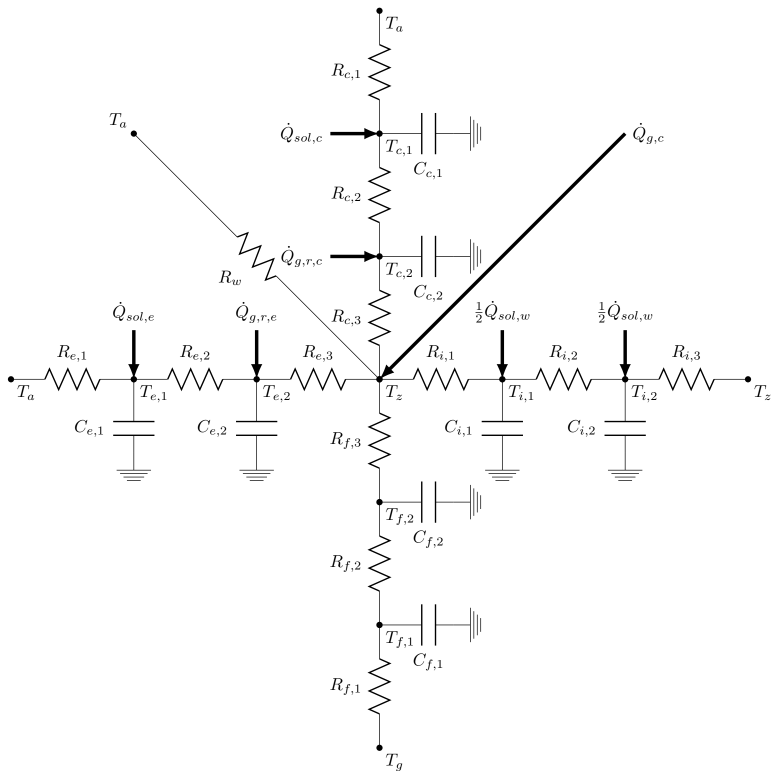

Figure 4. Twenty-one-parameter thermal RC network

When using the inverse gray-box modeling approach described in this work, questions naturally arise about the RC network structure that is most appropriate for the modeling task. Selecting a very complex model structure results in a difficult parameter estimation task, but too simple a model may not appropriately capture the desired dynamics. In this research the reduced-order modeling (ROM) environment was developed to allow for model structure flexibility, so this question may be investigated. As previously mentioned, various RC network forms have been considered in this work ranging from five to 21 parameters. Because the 21-parameter model was previously introduced, discussion will begin with the 18-parameter model (see Figure 5). This model can be considered a subset of the 21-parameter model with the internal surface heat transfer elements simplified to 1R1C. This reduced the parameter estimation procedure three parameters and kept most of the structure of the 21-parameter model. The 13-parameter model, shown in Figure 6, is also a subset of the 21-parameter model, with a simplified internal surface node and no ground heat transfer. The initial thought for this model is that for small footprint high-rise buildings the ground heat transfer may not be a significant contributor to the overall thermal load. Also a subset of the initial 21-parameter network, the 11-parameter model (Figure 7) contains the simplified internal surface network, as well as a simplified ground heat transfer network and lumped ceiling and exterior wall networks. The eight-parameter model, shown in Figure 8 further simplifies the 11-parameter model by neglecting ground heat transfer. This model contains a 3R2C network for exterior surfaces, a glazing resistance, and a simplified internal surface/mass network.

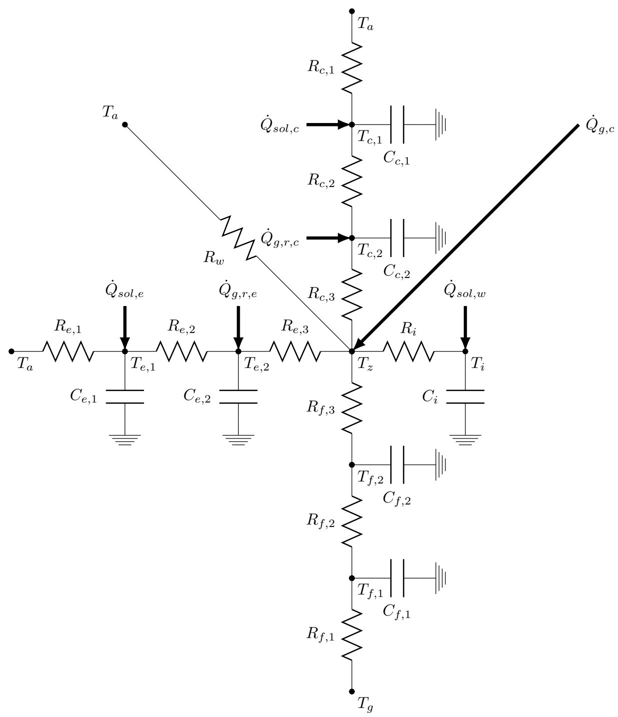

Figure 5. Eighteen-parameter thermal RC network

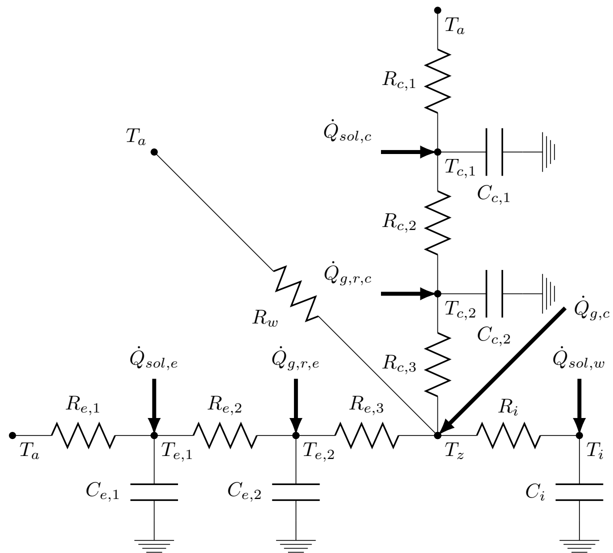

Figure 6. Thirteen-parameter thermal RC network

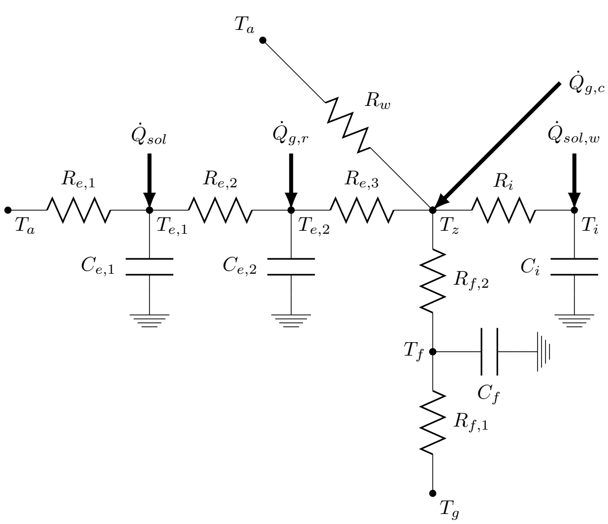

Figure 7. Eleven-parameter thermal RC network

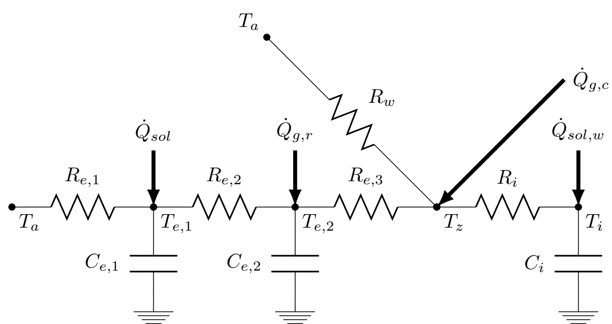

Figure 8. Eight-parameter thermal RC network

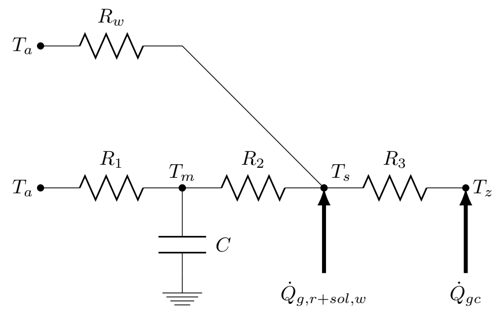

Figure 9. Five-parameter thermal RC network

In this work, we adopt a five-parameter single-zone model, shown in Figure 9; its structure was adapted from the thermal RC network used in the CEN-ISO 13790 "Simple Hourly Method" load calculations (ISO, 2007). Heat transfer and storage of opaque building shell materials are represented by R_1, R_2, and C. These elements link the ambient temperature node to a pseudo interior surface temperature node T_s, accounting for potential heat storage of the mass materials. Glazing heat transfer is represented by a single resistance R_w connecting the ambient temperature node to the surface temperature node, because thermal storage of glazing is typically neglected. R_3 represents a lumped convection/radiation coefficient between the surface temperature node and the zone air temperature node T_z. The convective portions of internal gains (lighting, occupants, and equipment) are applied as a direct heat source to the zone temperature node, shown as $\dot{Q}_{g,c}$, and the radiant fraction along with glazing transmitted solar gains $\dot{Q}_{g,r+sol,w}$ are applied to the surface node.

We decided to adopt the five-parameter thermal model after performing a model complexity analysis including all six thermal RC model structures previously presented. Each of the six RC networks (five-parameter, eight-parameter, 11-parameter, 13-parameter, 18-parameter, and 21-parameter) was trained using surrogate data from the five-zone U.S. Department of Energy Stand-alone Retail Reference EnergyPlus model. Table 2 summarizes the model performance in terms of root mean square error (RMSE) with respect to a validation dataset, and in terms of an objective generalized cross-validation score (GCV). GCV is defined in Equation 3.1 and essentially weights the mean-squared error based on model complexity (Bracken et al., 2010).

Obviously, the 11-parameter model is superior to the five-parameter model in terms of RMSE and GCV. Visual inspection, however, proved that the model responses in terms of zone temperature and sensible zone load are virtually identical; therefore, we chose to adopt the simpler five-parameter model to reduce sample size in the Monte Carlo analyses.

$$GCV = \frac{\sum_{i=1}^{N} \left(\dot{Q}_{rom,i} - \dot{Q}_{ep,i}\right)^2}{N\left(1-\frac{p}{N}\right)^2} \tag{3.1}$$

In Equation 3.1, N represents the total number of data points, $\dot{Q}_{rom,i}$ is the model predicted zone sensible load, $\dot{Q}_{ep,i}$ is the surrogate zone load, and p is the number of parameters in the model. The number of parameters p is equal to the number of RC parameters plus two, to account for the internal gain and zone capacitance multipliers that may also be used in model calibration.

For the retail building the 18-parameter model produced the lowest RMSE; however, the 21-parameter results were inadequate because they should have achieved at least the same score as the lower order model. The 11-parameter model produced the lowest GCV, which suggests that the additional improvement made by the 18-parameter model was not worth the additional complexity. Overall, the RMSE values for the retail building are all relatively low, further suggesting that all model forms performed well. Because satisfactory performance was observed from all models, the 5-parameter model was adopted to keep the problem dimensionality low.

Table 2. Model complexity results.

				Retail	
Model	p	N	k	RMSE	GCV
5p	7	504	128	6411	42.3×10^6
8p	10	504	1024	5338	29.7×10^6
11p	13	504	8192	3087	10.0×10^6
13p	15	504	32768	5234	29.1×10^6
18p	20	504	1048576	3076	10.3×10^6
21p	23	504	8388608	3192*	11.2×10^6

*Slightly suboptimal. Should have at least reached 3076 as the 18-parameter retail model.

A thermal RC network may be represented by a system of linear first-order differential equations with constant coefficients by performing an energy balance at each node with a storage element. This system can be represented in traditional state-space form as:

$$\dot{\mathbf{x}} = \mathbf{A}\mathbf{x} + \mathbf{B}\mathbf{u}$$
$$\mathbf{y} = \mathbf{C}\mathbf{x} + \mathbf{D}\mathbf{u}$$

For the five-parameter model adopted in the retail building modeling effort, state and input vectors are represented as:

$$\mathbf{x}^T = [T_m \;\; T_s]$$
$$\mathbf{u}^T = [T_z \;\; T_a \;\; \dot{Q}_{g,r+sol,w} \;\; \dot{Q}_{g,c}]$$

where T_m is the opaque building shell thermal temperature, T_s is the (pseudo) internal surface temperature, T_z is the zone temperature set point, T_a is the ambient external temperature,

$\dot{Q}_{g,r+sol,w}$ is the sum of the radiative portion of internal gains and the solar radiation transmitted through glazing, and $\dot{Q}_{g,c}$ is the total convective internal gains.

The state space equations are then converted to the following heat transfer function form:

$$\dot{Q}_{sh,t} = \sum_{k=0}^{n} \mathbf{S}_k^T \mathbf{u}_{t-k\Delta\tau} - \sum_{k=1}^{m} e_k \dot{Q}_{sh,t-k\Delta\tau} \tag{3.2}$$

where $\mathbf{S}$ is a matrix containing input coefficients, e_k is a vector containing heat gain history coefficients, n is the number of past inputs in the calculation, and m is the number of past heat gain values in the calculation.

The transfer function method is an efficient calculation routine as it relates the sensible heat gains to the space ($\dot{Q}_{sh}$) at time t to the inputs ($\mathbf{u}_t$) of n and heat gains ($\dot{Q}_{sh,t}$) of m previous time steps. The input weighting coefficients ($\mathbf{S}_k^T$) and zone load coefficients (e_k) are the results of the state space to transfer function conversion process described by Seem (Seem, 1987).

Performing an energy balance on the zone air node in Equation 3.3 provides a basis for sensible zone load calculations where C_z is the zone air (or node) capacitance, T_z is the zone air temperature node, $\dot{Q}_{sh,t}$ is the zone-sensible heat gain, $\dot{Q}_{inf}$ represents infiltration heat gain, and $\dot{Q}_{zs,t}$ is the required sensible zone load. In effect, the RC network model describes the transient heat transfer through opaque and transparent envelope components as well as internal gains from occupants, lighting, and equipment. This network is used to compute the heat gains from these sources to the air node. The complete energy balance is provided in Equation 3.3, including infiltration, zone air mass, and HVAC heat addition and extraction rates.

$$C_z \frac{dT_z}{dt} = \dot{Q}_{sh,t} + \dot{Q}_{zs,t} + \dot{Q}_{inf} \tag{3.3}$$

If the differential in Equation 3.3 is approximated by:

$$\frac{dT_z}{dt} \approx \frac{T_{z,t} - T_{z,t-\Delta}}{\Delta\tau}$$

it can be rearranged to develop an algebraic "inverse" transfer function for computing zone temperature predictions from a known zone load shown in Equation 3.4.

$$\bar{T}_z = \frac{\sum_{l=2}^{r} \mathbf{S}_0(l)\mathbf{u}_t(l) + \sum_{j=1}^{n} \mathbf{S}_j \mathbf{u}_{t-j\Delta\tau} - \sum_{j=1}^{m} e_j \dot{Q}_{sh,t-j\Delta\tau} + 2\frac{C_z}{\Delta\tau} T_{z,t-\Delta\tau} + \dot{m}_{inf} C_p \mathbf{u}_t(2) + \dot{Q}_{zs,t}}{2\frac{C_z}{\Delta\tau} - \mathbf{S}_0(1) + \dot{m}_{inf} C_p} \tag{3.4}$$

where r is the number of inputs in input vector $\mathbf{u}$, here $r = 4$. An assumption of this formulation is that the heat gains are computed using the average value over the time step so the actual temperature at a given time step can be determined from:

$$T_{z,t} = 2\bar{T}_{z,t} - T_{z,t-\Delta\tau}$$

An ideal load calculation scheme for a dual set point with a dead band scenario can be described by using the previous equations according to the following procedure:

for *t = simstart : simend* **do**
  Calculate $\dot{Q}_{sh,t}$ using Equation 3.2;
  Calculate $\dot{Q}_{zs,t}$ to maintain $T_z = T_{cool,set}$ using Equation 3.3 (assume cooling first);
  if $\dot{Q}_{zs,t} < 0$ *(heating required to maintain cooling set point)* **then**
    Set $\dot{Q}_{zs,t} = 0$. Compute floating temperature using Equation 3.4;
    if $T_z < T_{heat,set}$ **then**
      Recompute $\dot{Q}_{zs,t}$ to maintain $T_z = T_{heat,set}$ using Equation 3.3
    end
  end
end

To compute zone humidity, the simulation also includes a moisture balance as described in Equation 3.5:

$$m_{air}\frac{dW_Z}{dt} = \dot{m}_{inf}(W_{OA} - W_Z) + \dot{m}_{SA}(W_{SA} - W_z) + \frac{q_{occ,lat}}{h_{fg}} \tag{3.5}$$

where m_{air} is the mass of air in the zone, $\dot{m}_{inf}$ is the mass flow rate of air from infiltration, $\dot{m}_{SA}$ is the supply air (SA) mass flow rate, $q_{occ,lat}$ is the occupant latent gain, and h_{fg} is the heat of vaporization of water. W_z, W_{OA}, and W_{SA} are the humidity ratios of the zone, outdoor air, and SA, respectively.

3.1.3 Envelope Model Calibration

When using the inverse gray-box thermal modeling approach, it was necessary to determine the values of R and C parameters that bring the simple model into the closest agreement with the more detailed EnergyPlus model. Sum of squares minimization was used to identify model parameters that minimize the RMSE, defined by Equation 3.6, between the ROM predicted ($\dot{Q}_{rom}$) and the surrogate or measured ($\dot{Q}_{ep}$) sensible zone load.

$$J = \sqrt{\frac{\sum_{i=1}^{N}(\dot{Q}_{rom,i} - \dot{Q}_{ep,i})^2}{N}} \tag{3.6}$$

In this work, the two-stage optimization presented by Braun and Chaturvedi (2002) was implemented that first performs a direct search over the parameter space to identify a starting point for local refinement. The direct search is performed on k uniformly random points located within the bounds of the parameter space. The local refinement, subject to the same parameter constraints, is performed via nonlinear least squares minimization implemented using the MATLAB optimizer `lsqnonlin` based on trust-region Newton methods. The implementation in this environment also allows local refinement to be performed around several good starting points from the direct search. For higher complexity models the local optimization can be sensitive to the initial starting point. Good results have been found when the 12 best direct search points are given to separately executed least squares algorithms to simultaneously explore several attractive regions. Table 3 presents the calibrated parameters for the five-parameter model used throughout this work. The zone air capacitance multiplier CM represents furnishing and other mass associated with the air node; the internal gain multiplier scales the assumed internal gains from lights and equipment. These were considered the nominal parameter values to which uncertainty was applied later in the work.

Table 3. Calibrated Five-Parameter Network RC Parameters

Parameter	Value	Units
R_1	4.989	$(m^2K)/W$
R_2	0.164	$(m^2K)/W$
R_3	0.183	$(m^2K)/W$
R_w	3.000	$(m^2K)/W$
C	279.6	$kJ/(m^2K)$
CM	3.5	-
GM	0.788	-

3.1.4 HVAC System Modeling

For the standalone retail building a typical constant volume packaged rooftop unit (RTU) was modeled. Figure 10 provides an overview of the system configuration. The RTU model features a temperature- or enthalpy-based outdoor air economizer, constant-volume fan, single-speed direct expansion (DX) cooling coil, and gas heating coil. Component models were based on the quasi-steady-state physical formulations used by several mainstream whole-building simulation programs (Brandemuehl et al., 1993; DOE, 2010). Component models were programmed such that a full air loop can be simulated, allowing system air states to be included in a zone moisture balance for computing zone humidity levels.

Next, we assessed the fidelity of the new HVAC models against the EnergyPlus model. EnergyPlus outputs were used as inputs to the new HVAC models to compare with the HVAC system performance only. Comparing the EnergyPlus with the HVAC model implementations used in this work, Figures 11 and 12 show annual SA temperature and humidity ratio, respectively, for an annual simulation. In Figure 11, the top panel shows the SA temperature for occupied and unoccupied periods. To better visualize the information, weekly comparison plots are offered for a winter week and a summer week. Overall performance is very good during summer conditions. Mostly slight temperature deviations were noted during winter periods; however, early morning startup periods are visible where the ROM shows SA temperature values that are 10 K higher

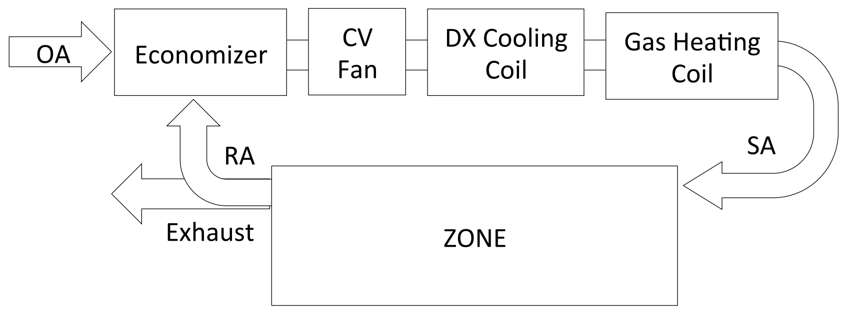

Figure 10. Packaged RTU

than the values found by EnergyPlus. After further review we discovered that this is an artifact of using average hourly rather than subhourly EnergyPlus outputs as validation data, and the fact that the ROM was simulated at hourly time steps.

During unoccupied periods the fan and heating coil cycle ran in unison to meet the required heating loads. During this operating mode the RTU model reports the SA temperature as the air temperature leaving the heating coil, which is near 50°Cwhen the coil is operating. In the case of the ROM, this temperature is reported for the entire hour even though the RTU does not run constantly for the hour. Because the EnergyPlus model was simulated at subhourly time steps, time intervals existed where they were not necessary for the heating coil and fan to run, and thus much lower supply temperatures were reported for some time steps. Thus, the hourly average SA temperature reported by EnergyPlus was 10 K lower. Had detailed (i.e., subhourly) EnergyPlus outputs been plotted for validation, several higher spikes near 50°Cwould have been observed along with lower values near 20°Cduring the hour.

Figures 13 and 14 highlight the calculated return air (RA) temperature and humidity ratio. Slight differences in the RA humidity can be observed in the results of the simplified zone moisture balance. As with SA temperatures, this is likely an artifact of using average hourly rather than subhourly EnergyPlus outputs as validation data. Simple first-order methods were used to implement the moisture balance and may also contribute to numerical differences between the two models. However, overall the model is a good approximation. Figures 15 and 16 show the predicted RTU energy consumption for an annual simulation; good results are observed for electricity and gas demand.

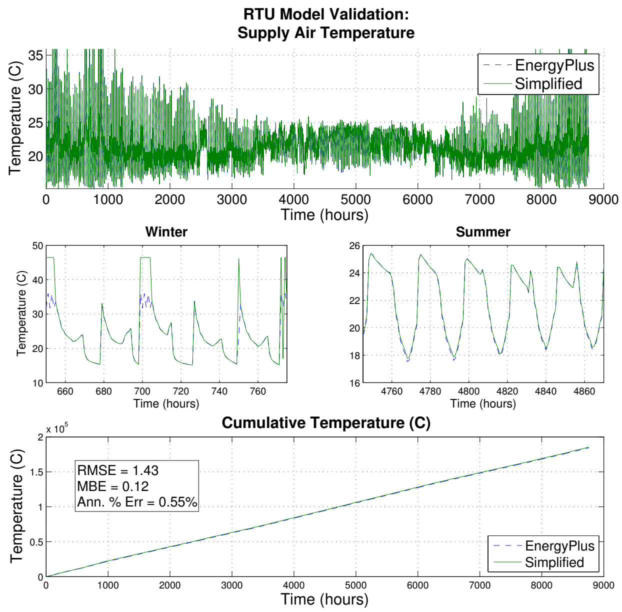

Figure 11. Validation of packaged RTU SA dry bulb temperature

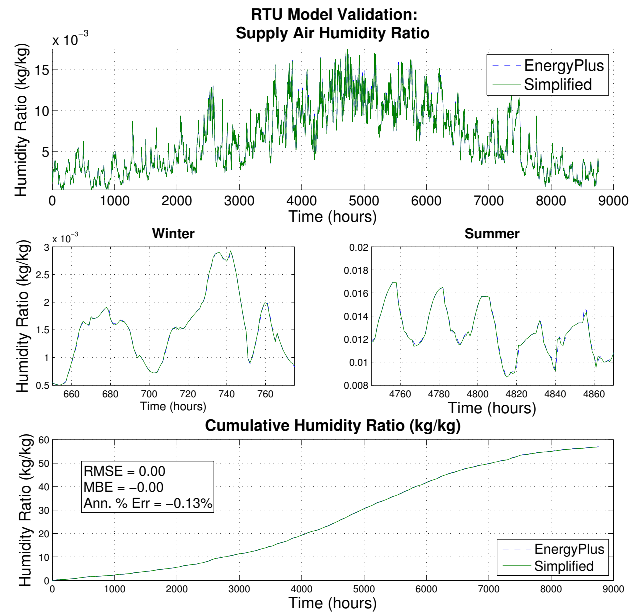

Figure 12. Validation of packaged RTU SA humidity ratio

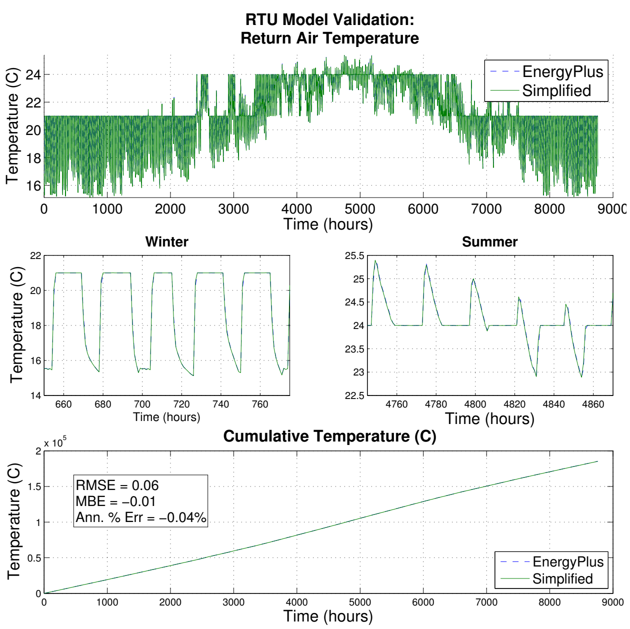

Figure 13. Validation of packaged RTU RA dry bulb temperature

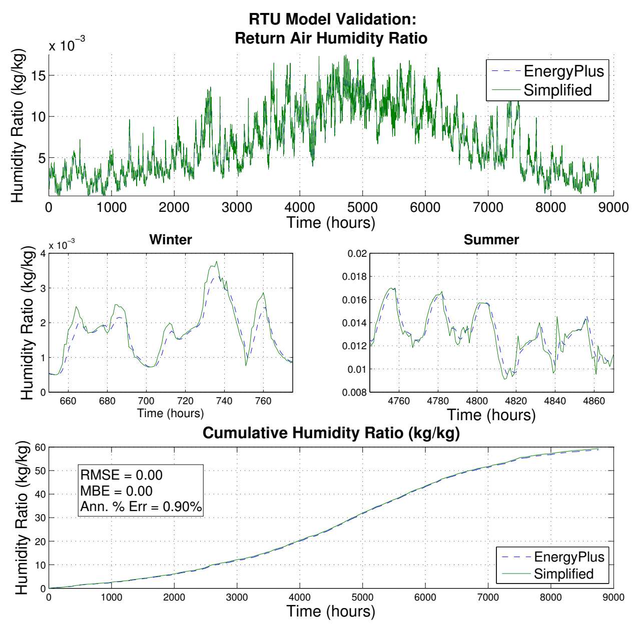

Figure 14. Validation of packaged RTU RA humidity ratio

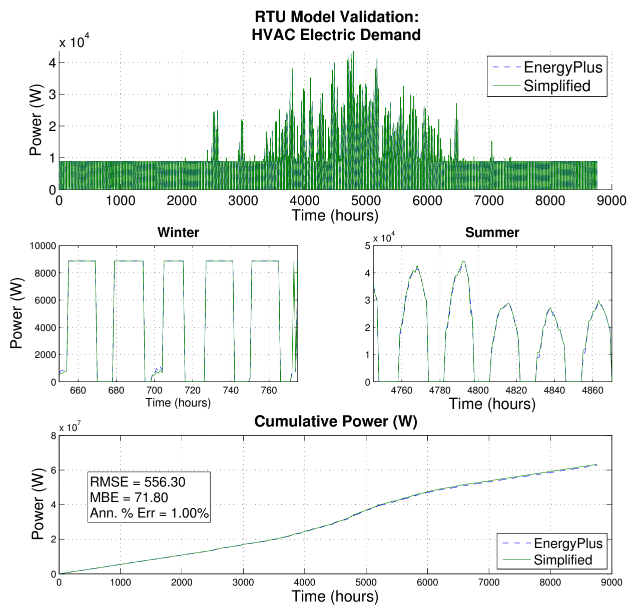

Figure 15. Validation of packaged RTU electricity demand

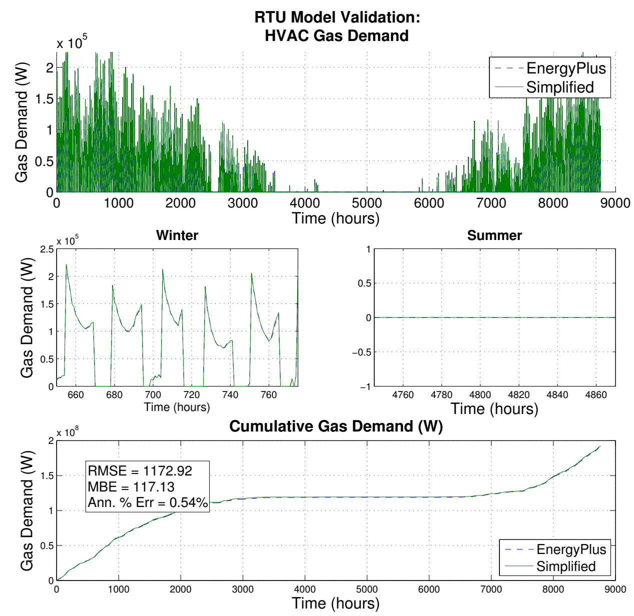

Figure 16. Validation of packaged RTU gas demand

3.1.5 Overall Retail Building Model Validation

The following results provide a comparison of overall gray-box retail building model performance compared to its five-zone EnergyPlus counterpart. That is, the RTU HVAC models described and validated in Section 3.1.4 were coupled to the five-parameter thermal RC network that was developed in Section 3.1.2 and calibrated in Section 3.1.3, to evaluate the ROM in its entirety. To provide better insight into the model performance under various conditions, we simulated it using typical nighttime setup (NSU) operation during a mild week and a precooling heuristic for a hot week. (These are validation time periods; i.e., neither was included in model calibration.) Sensible zone load, temperature, and HVAC electricity consumption are in fairly good agreement for NSU and the precooling scenarios in Figure 17 through 22.

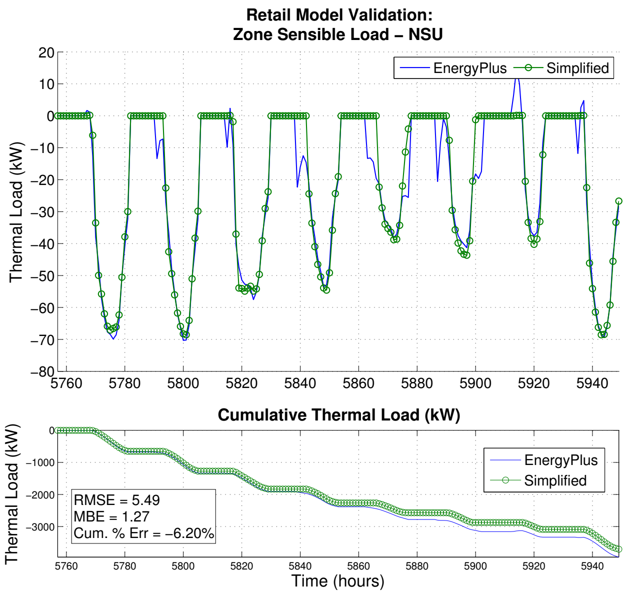

Figure 17. Retail sensible zone load comparison for NSU scenario

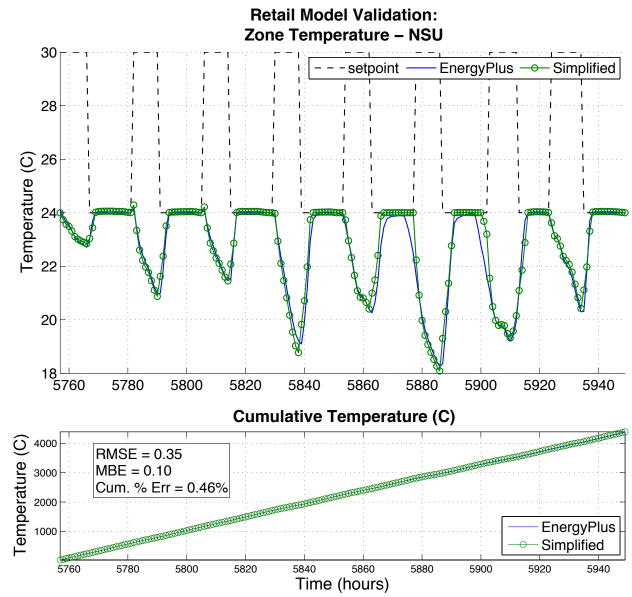

Figure 18. Retail zone mean air temperature comparison for NSU scenario

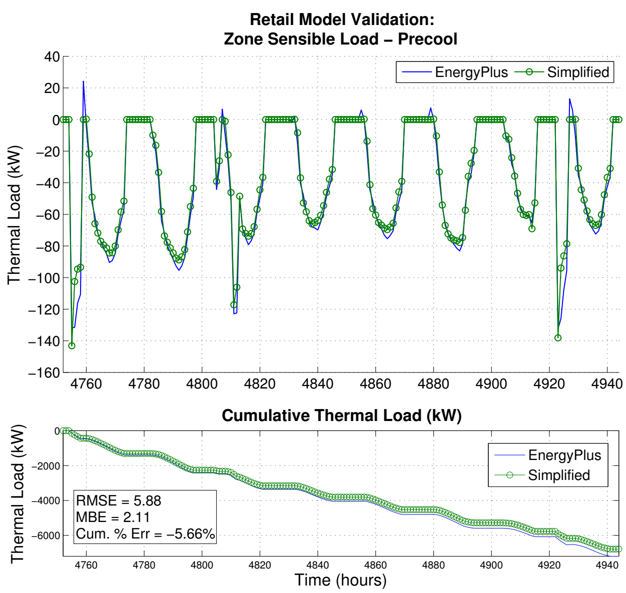

Figure 19. Retail sensible zone load comparison for precooling scenario

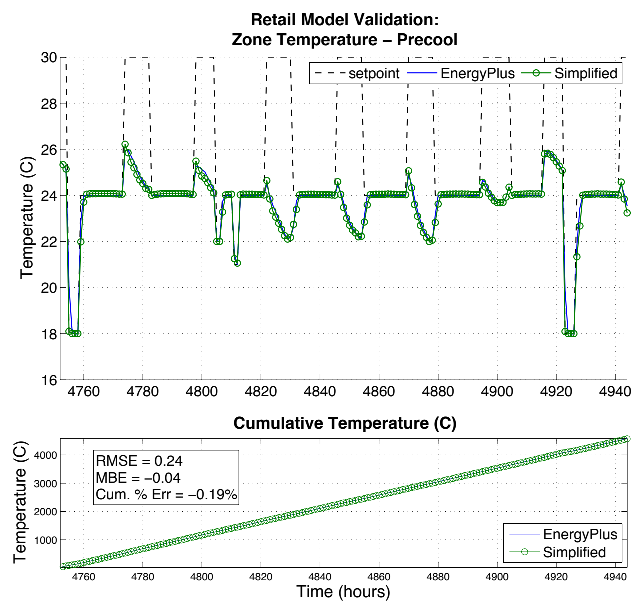

Figure 20. Retail zone mean air temperature comparison for precooling scenario

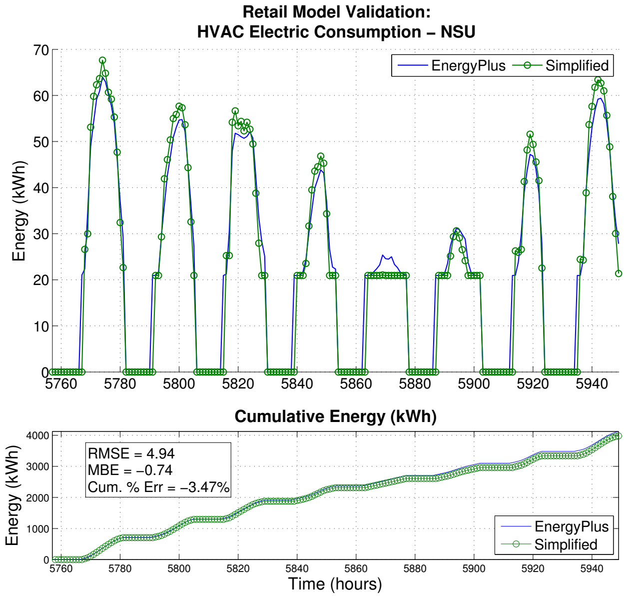

Figure 21. Retail HVAC electricity consumption comparison for NSU scenario

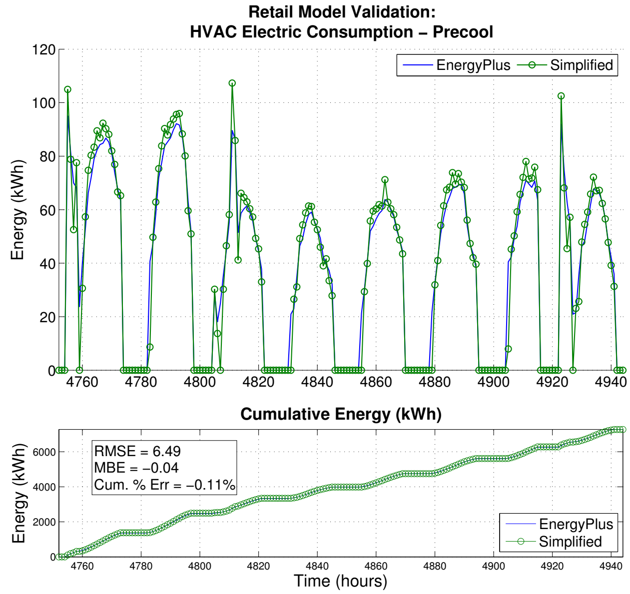

Figure 22. Retail HVAC electricity consumption comparison for precooling scenario

3.2 Uncertainty Quantification

To illustrate the capabilities of the energy signal tool, we adopted the five-parameter envelope (single-zone) ROM; its parameters were identified from hourly surrogate training data derived from an EnergyPlus simulation of a five-zone retail building near the Chicago Midway Airport. This model has five parameters for the building shell; however, 20 parameters are required for the building, its use, and HVAC systems; each parameter is considered to be uncertain.

3.2.1 Model Input Parameter Uncertainty

Input parameter distributions are characterized in this work using Gaussian distributions; faults are modeled with triangular distributions, although any other probability distribution may be selected. In this work, uncertainties are known varieties that are correctly quantified by an energy analyst using input distributions of choice; faults are effects of unobserved uncertainties that affect the measured building performance but not the modeled predictions.

The chosen distributions represent the best available knowledge of each uncertain model parameter. Input parameters are distributed around a mean that equals the nominal parameter value found from the parameter estimation process that has resulted in the validated ROM presented above. A standard deviation of 10% of the mean is adopted for the uncertain input parameters.

Adopting the five-parameter ROM, 11 parameters are associated with the building shell and use and an additional nine parameters are associated with the HVAC system. The seven nominal building envelope parameters are shown in Table 3, the four use parameters are shown in Table 4, and the nine nominal HVAC-related model parameters are shown in Table 5.

Table 4. Retail Building Use Parameters

Parameter	Value	Units
Lighting power density	32.30	W/m^2
Equipment power density	5.23	W/m^2
Occupant density	7.1	m^2/per
Infiltration flow rate	3.9	m^3/s

Table 5. Retail Building HVAC Parameters

Parameter	Value	Units
Supply fan efficiency	57	%
Maximum supply fan airflow	13.5	m^3/s
Supply fan pressure rise	883	Pa
DX coil rated capacity	319	kW
DX coil rated sensible heat ratio	70	%
DX coil rated coefficient of performance (COP)	3.2	-
DX coil rated air mass flow rate	16.0	kg/s
Gas heating coil-rated capacity	457	kW
Gas heating coil efficiency	80	%

To demonstrate the tool, five of the 20 input parameters are considered uncertain: lighting power density, equipment power density, occupant density, DX coil-rated COP, and gas heating coil efficiency. The remaining 15 input parameters are taken at their nominal values. In reality, most of these 20 parameters would be uncertain at different levels of uncertainty.

3.2.2 Operational and Equipment Faults

In spite of an energy analyst's best intentions and a belief that the model accurately reflects the building with all uncertainties, undetected faults may affect building performance. In this work, a fault differs from a parameter uncertainty in that it is present without the knowledge of the energy analyst or building operator; i.e., it is unobserved, yet still affects the measured conditional distributions of building energy end use.

We chose an additional six model parameters to represent such a faulted state. Tehse are modeled by triangular distributions, which may be asymmetrical. The outdoor air fraction's nominal value is 24.5%, but may vary from 0% to 100%. The airside economizer high limit temperature is nominally 28°C, but can vary between 12 and 40°C. Essentially, at very low values of the high limit temperature the economizer is disabled; at high values the economizer operation is not overridden. Heating and cooling temperature set points may differ from their assumed values with a random offset from -1.5 to +1.5 K. Moreover, the internal gains schedules may be expanded by up to 3 hours or contracted by up to 3 hours from the nominal building operation schedule. Finally, the schedules for internal gains from lighting and equipment may be shifted by up to 4 hours in each direction; i.e., to earlier and later onsets. Because the environment uses hourly time steps, the schedule contraction/expansion and shift are rounded to the nearest full hour. For the fault-free scenario the six fault parameters are kept at their nominal values. For the faulted case, all six fault parameters are randomly perturbed concurrently; i.e., a very wide range of fault combinations is explored.

Table 6. Fault Ranges

Parameter	Nominal	Minimum	Maximum	Units
Outdoor air fraction	24.5	0	100	%
Airside economizer high limit	28	12	40	°C
Cooling temperature set point	22.8	-1.5	+1.5	°C
Heating temperature set point	21.7	-1.5	+1.5	°C
Internal gains contraction/expansion	10	-3	+ 3	h
Internal gains shift	8:00 a.m. to 6:00 p.m.	-4	+ 4	h

Random sampling of 10,000 annual samples for each case is presented here. Because parameter combinations randomly drawn from the input distributions described above may lead to infeasible model configurations for which no solution can be computed, only valid model results are retained. The sample rejection was put in place to deal with parameter combinations that cause simulation errors such as non-convergence and subsequent crashes. Crashes are most often observed when randomly sampling a wide range of HVAC equipment-rated parameters, because the random sampling may not always produce physically consistent rated conditions. Thus, we expect that the wider the input parameter distributions, the more frequently invalid model results are generated. In the fault-free scenario 99.94% of all samples were valid (six of 10,000 failed); in the faulted scenario 99.88% of all samples were valid (12 of 10,000 failed).

The resultant conditional distribution of whole-building, HVAC, lighting (LTG), and plug electricity EQP consumption is shown in Figure 23; Table 7 shows pertinent statistics of the same in units of [MWh/a]. In the figure and table, whole-building electricity (WBE) please define and add to nomenclature is the sum of HVAC, LTG, and miscellaneous electric loads EQP. For fault-free and faulted cases, the table shows the mean, 10th, 50th (median), and 90th percentiles, along with the deterministic mean without consideration of any parameter uncertainty.

It is evident that the uncertainty associated with the five selected parameters only slightly affects the mean but strongly affects the variance in the whole-building and submetered end uses. The central 80% of the WBE consumption can be found within -7% and +8% from the deterministic mean in the fault-free case, and within -24% and +20% from the deterministic mean in the faulted case. The influence of faults is stronger in the HVAC and LTG end uses compared to the EQP end use. Given the dominance of HVAC and LTG end uses on whole-building consumption WBE, faults strongly affect WBE as well. Above all, faults widen the energy distributions.

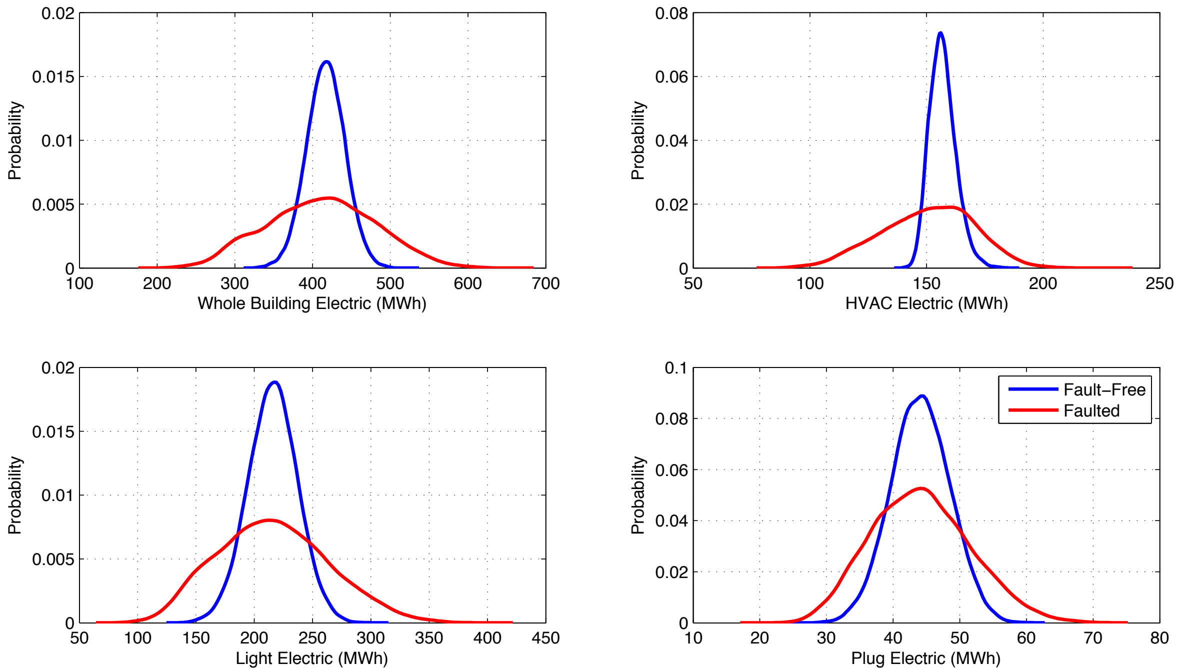

Figure 23. Distributions of whole-building, HVAC, lighting, and plug electricity consumption

Table 7. Summary Statistics of Conditional Distributions of Whole-Building, HVAC, Lighting, and Plug Electricity Consumption in [%] in [MWh/a]

			Percentile		
End-Use	Case	Mean	10th	50th	90th
WBE	Deterministic	416.3			
	Fault-free	100%	93%	100%	108%
	Faulted	99%	76%	99%	120%
HVAC	deterministic	156.5			
	Fault-free	100%	96%	100%	105%
	Faulted	96%	79%	97%	112%
LTG	deterministic	215.8			
	Fault-free	100%	87%	100%	113%
	Faulted	100%	71%	99%	130%
EQP	deterministic	44.1			
	Fault-free	100%	87%	100%	113%
	Faulted	100%	78%	100%	123%

3.3 Decision Analysis

Comparing monitored data against a probable range of expected energy use is more insightful than comparing against a single number, because it allows a building owner to assess the urgency of corrective actions that need to be taken. If the measured energy use lies at the edge of the probable range of expected values, given all the uncertainties in the model inputs, the owner can be very confident that an issue requires attention. In this work, a decision-making tool was developed based on the probability distribution of model predictions to determine the expected utility of a range of available decisions, suggesting the one that maximizes the expected utility. The tool takes on the form of a modified traffic light with red, yellow, and green lights. We adopted the perspective that a red light is shown both for high levels of overconsumption and high levels of underconsumption, because a building consuming significantly less energy than expected may indicate an operational problem as significant as a building consuming too much. A yellow signal is similarly used for cases of mild overconsumption and mild underconsumption. A green light is reserved for measured building energy consumption that is in line with model expectations.

As a first step, a distribution of the model-predicted energy consumption (called E_{mod}) was generated using Monte Carlo simulation as described in Section 3.2.

Second, the cases falling on the 5th, median, and 95th percentiles of the modeled energy distributions were selected to represent low, medium, and high estimates of actual measured energy consumption (called E_{meas}) for fault-free and faulted scenarios. The decision analysis compared the distribution of model-predicted energy consumption with E_{meas} to determine appropriate actions; thus, to illustrate the decision tool these three values of E_{meas} were taken from the sampled distributions. When physically implemented, the measured energy consumption would be determined directly from building metering data.

Third, boundaries were computed from the measured energy consumption to define meaningful ranges of low and high levels of deviation in energy consumption. Beginning with a low level of deviation, let us define $E_{0,low}$ such that it is X_{low} percent below E_{meas} and $E_{1,low}$ such that it is X_{low} percent above E_{meas}.

$$E_{0,low} = E_{meas}(1 - X_{low})$$
$$E_{1,low} = E_{meas}(1 + X_{low})$$

Similarly, for a high level of deviation, let's define $E_{0,high}$ such that it is X_{high} percent below E_{meas} and $E_{1,high}$ such that it is X_{high} percent above E_{meas}.

$$E_{0,high} = E_{meas}(1 - X_{high})$$
$$E_{1,high} = E_{meas}(1 + X_{high})$$

Of course, $X_{low} < X_{high}$ and we arbitrarily define X_{low} to be 5% and X_{high} to be 10%, i.e., a small deviation around the metered end use is $\pm 5\%$ and a large deviation $\pm 10\%$. It would be easy to adopt different values for X_{low} and X_{high} for each building energy end use depending on its temporal variability. Once we have a conditional probability distribution of expected energy consumptions in hand, we can make various kinds of statements. Here, we desire to report that the actual energy use is much higher, somewhat higher, similar, somewhat lower, or much lower than anticipated. We further want to assign costs to making correct and incorrect statements, and report the statement that has lowest expected cost.

Fourth, the empirical cumulative distribution of expected energy consumption was used to find the cumulative probabilities for the anticipated energy consumption to be below $E_{0,high}$ (called P_1), between $E_{0,high}$ and $E_{0,low}$ (called P_2), between $E_{0,low}$ and $E_{1,low}$ (called P_3), between $E_{1,low}$ and $E_{1,high}$, (called P_4) and above $E_{1,high}$ (called P_5). Together, these probabilities form the state probability vector $\vec{P} = (P_1, P_2, P_3, P_4, P_5)^T$ as shown in Figure 24.

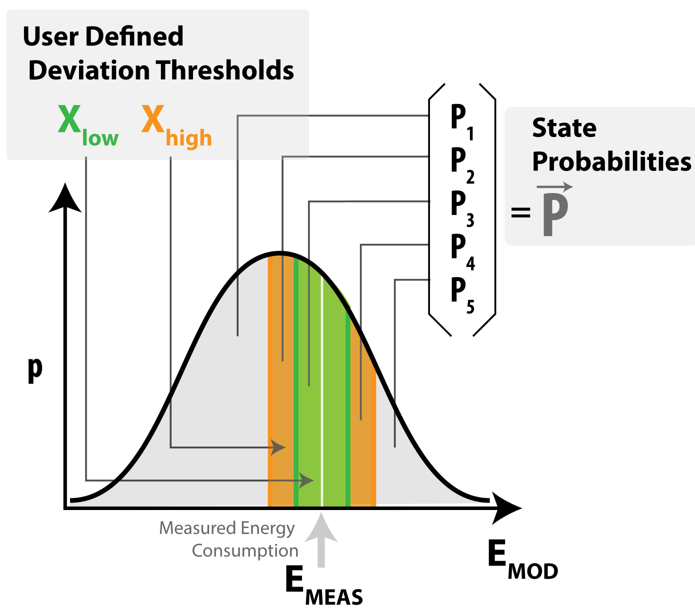

Figure 24. Relationship between deviation thresholds X_{low} and X_{high} and state probability vector $\vec{P}$

Fifth, we define a cost function K, where cost is a function of state and action with a finite number of states and a finite number of actions. Therefore, this cost function can be represented as a matrix. Let us agree that there is one row per action and one column per state $K(i, j)$; i.e., cost of action i in state j. Let action $i = 1$ display the lower red light (RL) on the modified traffic signal, action $i = 2$ the lower yellow (YL) signal, $i = 3$ a green (G) signal, action $i = 4$ the upper yellow (YH) signal, and finally $i = 5$ be displaying the upper red (RH) light. Let $j = 1$ be the state that the model predicts a much lower (ML) energy consumption, $j = 2$ a somewhat lower (SL) energy consumption, $j = 3$ about the same (S), $j = 4$ a somewhat higher (SH) energy consumption, and $j = 5$ a much higher (MH) energy consumption than the actual building. Action vector $\vec{a}$ has thus five elements.

Table 8. Decision Analysis State and Action

	State j: Anticipated Model Energy				
Action i:	Much Lower	Somewhat Lower	Similar	Somewhat Higher	Much higher
Lower red	K(RL,ML)	K(RL,SL)	K(RL,S)	K(RL,SH)	K(RL,MH)
Lower yellow	K(YL,ML)	K(YL,SL)	K(YL,S)	K(YL,SH)	K(YL,MH)
Central green	K(G,ML)	K(G,SL)	K(G,S)	K(G,SH)	K(G,MH)
Upper yellow	K(YH,ML)	K(YH,SL)	K(YH,S)	K(YH,SH)	K(YH,MH)
Upper red	K(RH,ML)	K(RH,SL)	K(RH,S)	K(RH,SH)	K(RH,MH)

An advantage of the presented decision analysis tool lies in its ability to individually set the costs of actions given certain states. Here, we make reasonable but somewhat arbitrary assumptions on the values of the cost matrix elements: Showing an RL light when the model predicts ML energy consumption is assumed to have a cost of 4 (strong false negative, lost savings opportunity), when the model predicts an SL energy consumption a cost of 3 (false negative), when the model predicts a similar energy consumption a cost of 2 (weak false negative), when the model predicts an SH energy consumption a cost of 1 (weak false negative), and finally, when the model predicts MH energy consumption a cost of 0 (correct identification). Showing an RH light when the model predicts ML energy consumption is assumed to have a cost of 0 (correct identification), when the model predicts an SL energy consumption a cost of 1 (weak false positive), when the model predicts a similar energy consumption a cost of 2 (weak false positive), when the model predicts an SH energy consumption a cost of 3 (false positive), and finally, when the model predicts MH energy consumption a cost of 4 (strong false positive, unnecessary alarm). Similar arguments can be made for the remaining signals of a lower yellow (YL), a green, and an upper yellow (YH) light, and we yield the following cost matrix.

$$
\begin{aligned}
K &= \begin{bmatrix} K(RL,ML) & K(RL,SL) & K(RL,S) & K(RL,SH) & K(RL,MH) \\ K(YL,ML) & K(YL,SL) & K(YL,S) & K(YL,SH) & K(YL,MH) \\ K(G,ML) & K(G,SL) & K(G,S) & K(G,SH) & K(G,MH) \\ K(YH,ML) & K(YH,SL) & K(YH,S) & K(YH,SH) & K(YH,MH) \\ K(RH,ML) & K(RH,SL) & K(RH,S) & K(RH,SH) & K(RH,MH) \end{bmatrix} \\
&= \begin{bmatrix} 4 & 3 & 2 & 1 & 0 \\ 3 & 2 & 1 & 0 & 1 \\ 2 & 1 & 0 & 1 & 2 \\ 1 & 0 & 1 & 2 & 3 \\ 0 & 1 & 2 & 3 & 4 \end{bmatrix}
\end{aligned} \tag{3.7}
$$

The expected cost vector for each action is found by multiplying the cost matrix K with the probability vector $\vec{P}$:

$$E(\vec{a}) = K \cdot \vec{P}$$

$$
\begin{bmatrix} E(RL) \\ E(YL) \\ E(G) \\ E(YH) \\ E(RH) \end{bmatrix} = \begin{bmatrix} K(RL,ML) & K(RL,SL) & K(RL,S) & K(RL,SH) & K(RL,MH) \\ K(YL,ML) & K(YL,SL) & K(YL,S) & K(YL,SH) & K(YL,MH) \\ K(G,ML) & K(G,SL) & K(G,S) & K(G,SH) & K(G,MH) \\ K(YH,ML) & K(YH,SL) & K(YH,S) & K(YH,SH) & K(YH,MH) \\ K(RH,ML) & K(RH,SL) & K(RH,S) & K(RH,SH) & K(RH,MH) \end{bmatrix} \begin{bmatrix} P_1 \\ P_2 \\ P_3 \\ P_4 \\ P_5 \end{bmatrix}
$$

$$
= \begin{bmatrix} K(RL,ML)P_1 + K(RL,SL)P_2 + K(RL,S)P_3 + K(RL,SH)P_4 + K(RL,MH)P_5 \\ K(YL,ML)P_1 + K(YL,SL)P_2 + K(YL,S)P_3 + K(YL,SH)P_4 + K(YL,MH)P_5 \\ K(G,ML)P_1 + K(G,SL)P_2 + K(G,S)P_3 + K(G,SH)P_4 + K(G,MH)P_5 \\ K(YH,ML)P_1 + K(YH,SL)P_2 + K(YH,S)P_3 + K(YH,SH)P_4 + K(YH,MH)P_5 \\ K(RH,ML)P_1 + K(RH,SL)P_2 + K(RH,S)P_3 + K(RH,SH)P_4 + K(RH,MH)P_5 \end{bmatrix} \tag{3.8}
$$

As suggested by utility theory, the last step is to select the best action a_{opt} in the face of uncertainty; i.e., activate that light, which minimizes the expected cost.

$$
a_{opt} = \operatorname*{argmin}_i E(\vec{a})
$$

3.4 Bayesian Updating

Thus far, the distributions of the uncertain model parameters were assumed to be Gaussian with a standard deviation equal to a fixed fraction of the parameter mean, here 10%. The choice of these distributions was made somewhat arbitrarily, before any operational data was available from the actual building performance and termed before data because of its consideration prior to observation. We believe that building performance measurements collected over an extended time period (i.e., after data) can be used to infer improved input parameter distributions by applying probability theory in general and Bayes' theorem in particular. See Jaynes (Jaynes, 2003) for full development of Bayesian probability. A brief explanation is provided below for information pertinent to this research.

High-dimensional integrals associated with problems in computational physics lead to the development of Markov Chain Monte Carlo algorithms, which can efficiently sample from probability distributions by exploiting the Markov property. This has led to the explosion of Bayesian techniques, with the Metropolis Algorithm as the breakthrough approach (named as one of the top 10 algorithms of the 20th century) (Cipra, 2000). A probabilistic perspective not only provides insight into the relationship between sets of model parameters, revealing tradeoffs and compensating interactions, but also lends itself to a continuous model uncertainty quantification and tuning where the posterior distribution of an initial parameter estimate can be used as the prior for a subsequent parameter estimation update once new building performance data have been collected.

Dodier used Bayesian (belief) networks for whole-building energy diagnostics (Dodier and Kreider, 1999; Dodier et al., 1998). Lauret et al. (2006) demonstrated improvements over traditional parameter estimation methods by applying Bayes' theorem to determine better estimates of convection coefficients for a radiant barrier roof system model. More recently, Booth et al. (2012)

used London housing stock models for hierarchical modeling, with considerations of internal heating set points, fraction of space heating, air leakage, heating system COP, window U-value, and window-to-wall ratio.

In this work, the Bayesian inference of uncertain model parameters relies on the extension of a previously developed technique (Neumann et al., 2011). It has benefits over traditional methods because prior knowledge of the system can be directly incorporated into the estimation task and methods for addressing sensor noise are inherent to the Bayesian approach. The inference can essentially be thought of as fitting a joint probability distribution to a measured dataset. Specifically, conditional probabilities are related through the product rule to derive Bayes' theorem and allow consideration of "before data" and "after data" states of knowledge. The prior probability distribution is updated with any measured data to form the posterior probability distribution, which represents the state of knowledge in any inference task. We propose a periodic process where model input parameter distributions are updated daily, weekly, monthly, or for a similar period of interest. As new measurements become available, data effectively shape the distribution of expected building energy use according to the information gleaned from a combination of prior knowledge and sensor data; uncertainty is still present but should decrease with additional data and understanding of the relationships among variables.

The probability of parameter set Θ given measured data D and knowledge of the system K can be written as posterior probability $p(\Theta|DK)$. Bayes' theorem then allows the conditional probability $p(\Theta|DK)$ to be computed from $p(\Theta|K)$, $p(D|\Theta K)$, and $p(D|K)$ as shown in Equation 3.9,

$$p(\Theta|DK) = p(\Theta|K)\frac{p(D|\Theta K)}{p(D|K)} \tag{3.9}$$

where $p(\Theta|K)$ represents prior knowledge about parameter values, $p(D|\Theta K)$ represents the likelihood of observing the measured dataset D given a particular parameter set Θ and knowledge of the system K, and $p(D|K)$ is the probability of observing the dataset. Ignoring the reference to system knowledge K, the relation can be written in alternate form where the numerator remains the product of likelihood and prior, and the denominator is a normalization factor so that posterior probabilities sum to unity.

$$p(\Theta|D) = \frac{p(\Theta)p(D|\Theta)}{\sum\limits_i p(\Theta_i)p(D|\Theta_i)} \tag{3.10}$$

Assuming random Gaussian noise about a measured datum D_i, the likelihood of an observation can be determined from its location within the normal distribution with standard deviation σ_ε this is not in nomenclature, centered at μ equal to the measured datum,

$$p(D_i|\Theta) = \frac{1}{\sigma_\varepsilon\sqrt{2\pi}}\exp\left(\frac{-(D_i - M_i)^2}{2\sigma_\varepsilon^2}\right), \tag{3.11}$$

where M_i is the model output given the parameter set Θ.

Further, assuming independent errors, the likelihood is that the entire dataset is simply the product of the likelihoods of all individual points. The assumption is likely valid for common HVAC sensors (e.g., temperature probes), but correlated errors could be handled with a slightly different formulation that is indicative of a fault model. Measurement errors are often correlated because of, for example, hysteresis error or linearity error. If such correlated errors are of concern, a Bayesian (or other probabilistic) method may be used that can accommodate correlated measurements. This work nonetheless assumes uncorrelated energy consumption measurements; thus, it ignores autocorrelation of errors, which is estimated to be small. For the dynamics and time range considered in this problem, model structure is considered more important, with respect to data fit, than noise correlation. From this model assumption, we derive the easily computable likelihood function given by Equation 3.12.

The likelihood function is maximized when the exponential term is minimized, which occurs as the modeled data approach the measured (or surrogate) data. When uniform priors are used with Equation 3.12 in a Bayesian calibration context, the most likely parameters are equivalent to those that would be found using a least squares approach, because the exponential term in Equation 3.12 is essentially the sum of squared errors (Pavlak et al., 2014).

$$p(D|\Theta) = \frac{1}{\left(\sigma_\varepsilon\sqrt{2\pi}\right)^n} \exp\left(\frac{-1}{2\sigma_\varepsilon^2}\sum_{i=1}^{n}(D_i - M_i)^2\right) \tag{3.12}$$

Evaluating Equation 3.12 directly can pose numerical issues, because a small range of σ_ε values results in a large range of likelihoods. Double precision computing environments are typically capable of evaluating floating point numbers on the order of 10^{-308} to 10^{308}. This means that when using 3 weeks of hourly data (i.e., $n = 504$), σ_ε must approximately be in the range of $[0.1, 1.5]$. Values outside this range will cause the likelihood (and consequently the posterior) to evaluate to "Inf," "NaN," or "0," regardless of the time series fit. These numerical issues can be alleviated by computing the natural logarithm of the posterior rather than the posterior directly (Lauret et al., 2006; Sivia and Skilling, 2006).

To compute the natural log of the posterior, first, the log of both sides of Equation 3.10 is taken.

$$\ln\left(p(\Theta|D)\right) = \ln\left(\frac{p(\Theta)p(D|\Theta)}{\sum_i p(\Theta_i)p(D|\Theta_i)}\right) \tag{3.13}$$

The right-hand side of Equation 3.13 can be separated using logarithm product and quotient rules.

$$\ln\left(p(\Theta|D)\right) = \ln\left(p(\Theta)\right) + \ln\left(p(D|\Theta)\right) - \ln\left(\sum_i p(\Theta_i)p(D|\Theta_i)\right) \tag{3.14}$$

The log-likelihood term of Equation 3.14,

$$\ln\left(p(D|\Theta)\right) = \ln \quad \frac{1}{\left(\sigma_\varepsilon\sqrt{2\pi}\;^{n}} \exp \quad \frac{-1}{2\sigma_\varepsilon^2}\sum_{i=1}^{n}\left(D_i - M_i\right)^2 \tag{3.15}$$

can be further simplified by applying product and quotient rules as shown in Equations 3.16 and 3.17, respectively.

$$\ln\left(p(D|\Theta)\right) = \ln \quad \frac{1}{\left(\sigma_\varepsilon\sqrt{2\pi}\;^{n}} \quad + \ln \quad \exp \quad \frac{-1}{2\sigma_\varepsilon^2}\sum_{i=1}^{n}\left(D_i - M_i\right)^2 \tag{3.16}$$

$$\ln\left(p(D|\Theta)\right) = \ln\left(1\right) - \ln\left(\left(\sigma_\varepsilon\sqrt{2\pi}\right)^{n}\right) + \ln \quad \exp \quad \frac{-1}{2\sigma_\varepsilon^2}\sum_{i=1}^{n}\left(D_i - M_i\right)^2 \tag{3.17}$$

With $\ln(1) = 0$, and the power rule can be applied to the middle term of the right-hand side. The last term of the right-hand side simplifies, because of to logarithmic identity, to produce Equation 3.18.

$$\ln\left(p(D|\Theta)\right) = -n\ln\left(\sigma_\varepsilon\sqrt{2\pi}\right) + \frac{-1}{2\sigma_\varepsilon^2}\sum_{i=1}^{n}\left(D_i - M_i\right)^2 \tag{3.18}$$

Recombining the simplified log-likelihood of Equation 3.18 with the log-posterior equation of Equation 3.14 yields:

$$\begin{aligned}\ln\left(p(\Theta|D)\right) = \ln\left(p(\Theta)\right) - n\ln\left(\sigma_\varepsilon\sqrt{2\pi}\right) - \frac{1}{2\sigma_\varepsilon^2}\sum_{i=1}^{n}\left(D_i - M_i\right)^2 \\ - \ln \quad \sum_{i} p(\Theta_i)p(D|\Theta_i)\end{aligned} \tag{3.19}$$

The last term of the right-hand side of Equation 3.19 is ultimately a constant number subtracted from each individual $\ln(p(\Theta_i)p(D|\Theta_i))$ value. Because the value of this constant term does not impact the shape or relative information of the posterior, it could be thought of as an arbitrary constant C.

$$\ln\left(p(\Theta|D)\right) = \ln\left(p(\Theta)\right) - n\ln\left(\sigma_\varepsilon\sqrt{2\pi}\right) - \frac{1}{2\sigma_\varepsilon^2}\sum_{i=1}^{n}\left(D_i - M_i\right)^2 + C \tag{3.20}$$

The constant term can be moved to the left-hand side of the equation, producing Equation 3.21.

$$\ln\left(p(\Theta|D)\right) - C = \ln\left(p(\Theta)\right) - n\ln\left(\sigma_\varepsilon\sqrt{2\pi}\right) - \frac{1}{2\sigma_\varepsilon^2}\sum_{i=1}^{n}\left(D_i - M_i\right)^2 \tag{3.21}$$

Because the objective is to avoid numerical underflow or overflow, prescribing

$$C = \max \quad \ln\left(p(\Theta)\right) - n\ln\left(\sigma_\varepsilon\sqrt{2\pi}\right) - \frac{1}{2\sigma_\varepsilon^2}\sum_{i=1}^{n}\left(D_i - M_i\right)^2 \tag{3.22}$$

shifts all points so that the maximum is 0. A maximum value of 0 in the ln space ensures that all values will be mapped to the interval $[0,1]$ when taking the exponential. After taking exponentials, the values can be scaled by a constant so that probabilities sum to unity.

The σ_ε value is a noise term with physical interpretation. Here there are three energy signals of interest: HVAC, lighting, and equipment–all electrical terms with the error associated with minor fluctuations not incorporated in the physical model. As previously stated, prescribing an appropriate σ_ε is necessary to prevent underflow or overflow, which causes the inference task to crash from numerical issues. The most appropriate σ_ε value can be found by maximum a posteriori (MAP) estimation. MAP is used to obtain a point estimate of σ_ε by placing a prior distribution over σ_ε and finding the maximum posterior mode according to the empirical data. Because the HVAC, lighting, and equipment energy signals are considered independent in this study, the MAP estimate of $\sigma_{\varepsilon,\,HVAC}$, $\sigma_{\varepsilon,\,LTG}$, and $\sigma_{\varepsilon,\,EQP}$ were performed separately with a uniform prior on each σ_ε set between 0% and 15% of the magnitude of the full, individual signals.

With the appropriate and optimal σ_ε set for each signal, it was then possible to calculate the probability of observing various energy signals as a function of the uncertainty parameters. Because the signals are considered independent, the joint probability of the building state is a product of the individual probabilities:

$$p = \prod_i p_i = p_{HVAC}\, p_{LTG}\, p_{EQP}. \tag{3.23}$$

With the joint posterior probability distribution available from the equation above, it was then possible to sample from the posterior directly or marginalize over all parameters not of interest and form a new prior. That is, the updating process is *prior* $\rightarrow$ *posterior* $\rightarrow$ *prior*. The optimal updating period is a function of the building energy dynamics and available data.

4 Results

Results are presented that (1) exemplify the decision support aspect of the tool; and (2) illustrate the updating of the uncertain model parameters based on measured data.

4.1 Decision Support Case Studies

The decision analysis results presented here are separated into fault-free and faulted scenarios. In the fault-free scenario, the high, medium, and low consumption values (surrogates of measured building energy consumption) are drawn from the conditional energy consumption distributions without faults and the decision analysis is based on the same distribution. In contrast, in the faulted scenario, the high, medium, and low consumption values are drawn from the conditional energy consumption distributions *including faults* and the decision analysis is based on the distribution *excluding faults*.

The results are shown as a matrix of figures. The first row shows the whole-building electricity WBE consumption results for the last year, then last month, then last week, followed by the last day. The second row shows the HVAC energy consumption results for the time periods, the third row shows the lighting LTG results, and lastly, the fourth row shows the EQP results. Each of the 16 figure panels reveals a box plot[1] Larger and smaller values, respectively, are shown as outliers of the expected energy consumption value for the time period of interest, a diamond marker superimposed on the box plot to indicate the surrogate actual consumption value E_{meas}, and on the left margin the energy signal tool with the signal chosen for the resultant cumulative probabilities $\vec{P}$, cost matrix C, and deviation thresholds X_{low} and X_{high}. The central green light separates cases of mild (YH) and strong (RH) overconsumption above the green light from the cases of of mild (YL) and strong (RL) underconsumption below the green light. The particular traffic signal-inspired design is one of many possible designs chosen for illustration here; thus, many other valid designs can be conceived. Moreover, the planned field implementation of this energy signal tool would likely not show the box plots but only the signals. Finally, if only whole-building energy WBE measurements are available, the tool would reveal only the top row of WBE versus the four time periods. In contrast, when submetering of HVAC, LTG, and EQP is available, the lower three rows would be shown and the top WBE row omitted, because it would not offer additional insight.

[1]Box plots shown in this report adopt the common notation that the box occupies the interquartile range (IQR) from the lower (25th percentile) to the upper (75th percentile). The whiskers extend to the minimum and maximum values if these are less than 1.5 times the IQR below the lower or 1.5 times the IQR above the upper quartile.

4.1.1 Fault-Free Scenario

4.1.1.1 High Energy Consumption Case

Beginning on August 30 with the high energy consumption case at the 95th percentile, a mild overconsumption is shown for all time scales for WBE and HVAC; LTG and EQP show strong overconsumption for all time scales.

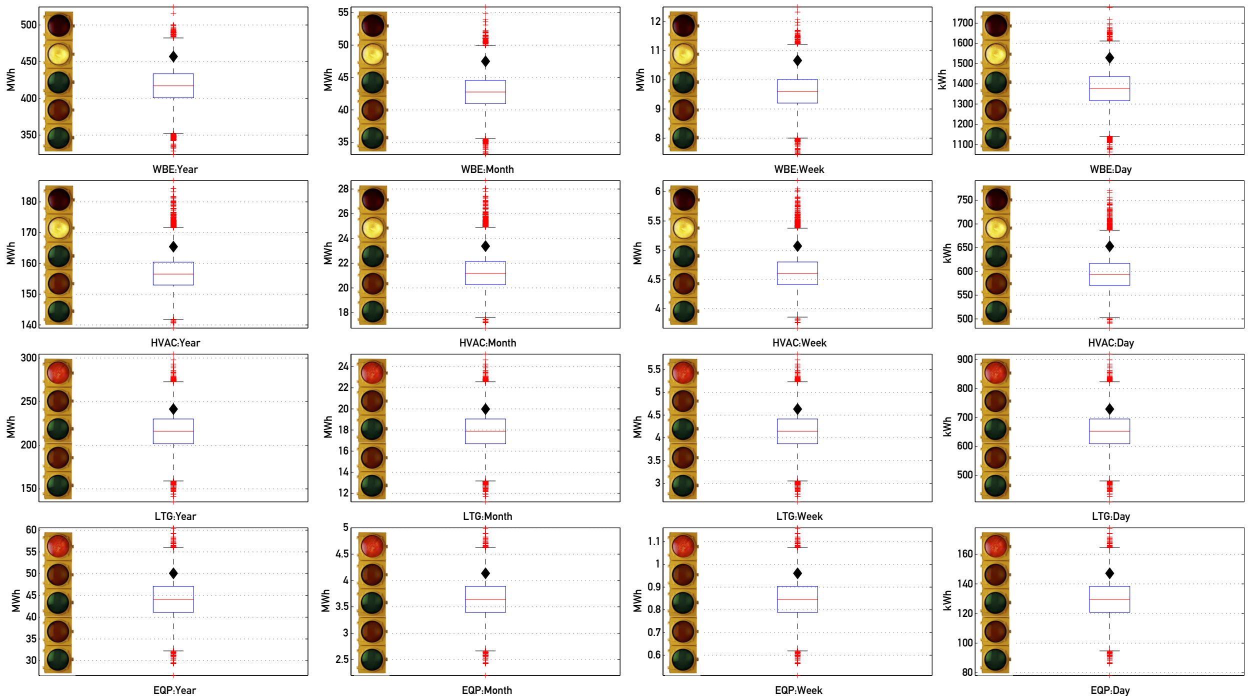

Figure 25. Fault-free high consumption case beginning August 30 (measured consumption data are indicated by diamonds in each figure)

4.1.1.2 Medium Energy Consumption Case

The medium consumption cases for August and February show consistency between WBE, HVAC, and LTG; green lights are shown for all time scales and the EQP consumption is low. Because the EQP contribution to the total is small, the WBE signal is not swayed to show a low yellow light.

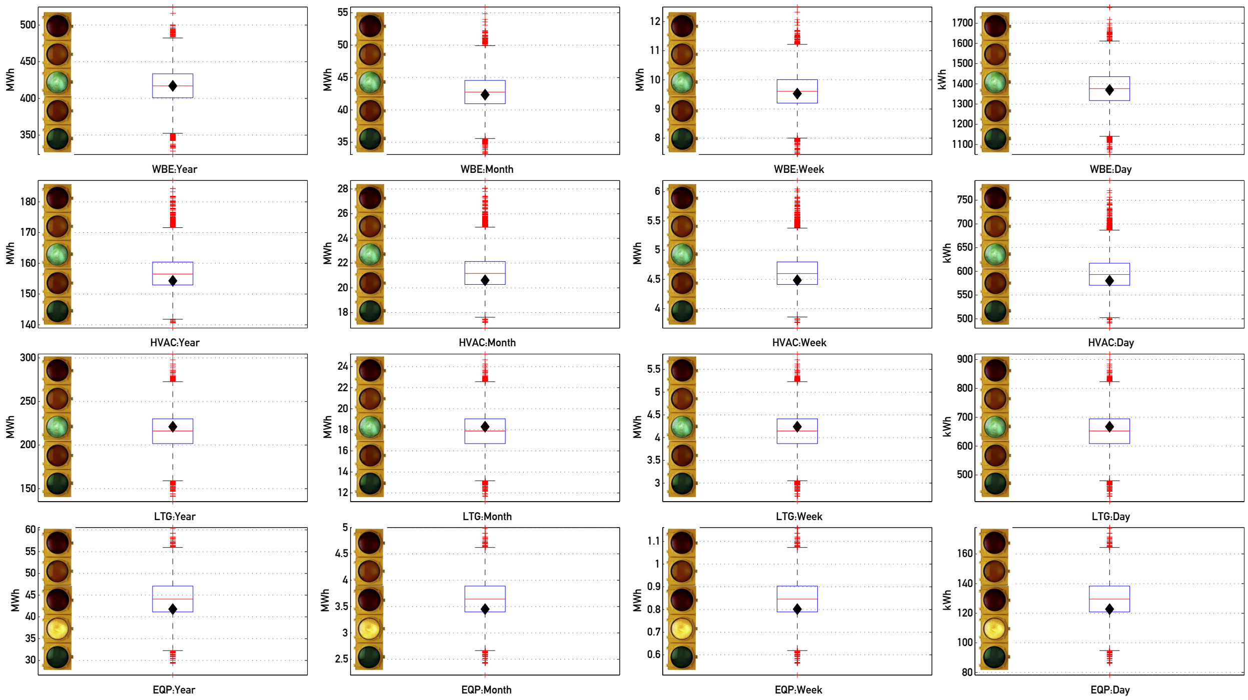

Figure 26. Fault-free medium consumption case beginning August 30 (measured consumption data are indicated by diamonds in each figure)

4.1.1.3 Low Energy Consumption Case

In the low consumption case, it is interesting to note that the WBE signal shows a strong underconsumption (low red), driven by the corresponding LTG signal, even though HVAC consumption is similar to the model expectation (green) and EQP is only a mild underconsumption. This case reveals the importance of submetering: Without it, it would not have been possible to isolate that LTG causes the warning, HVAC could be ignored, and EQP could be given less consideration.

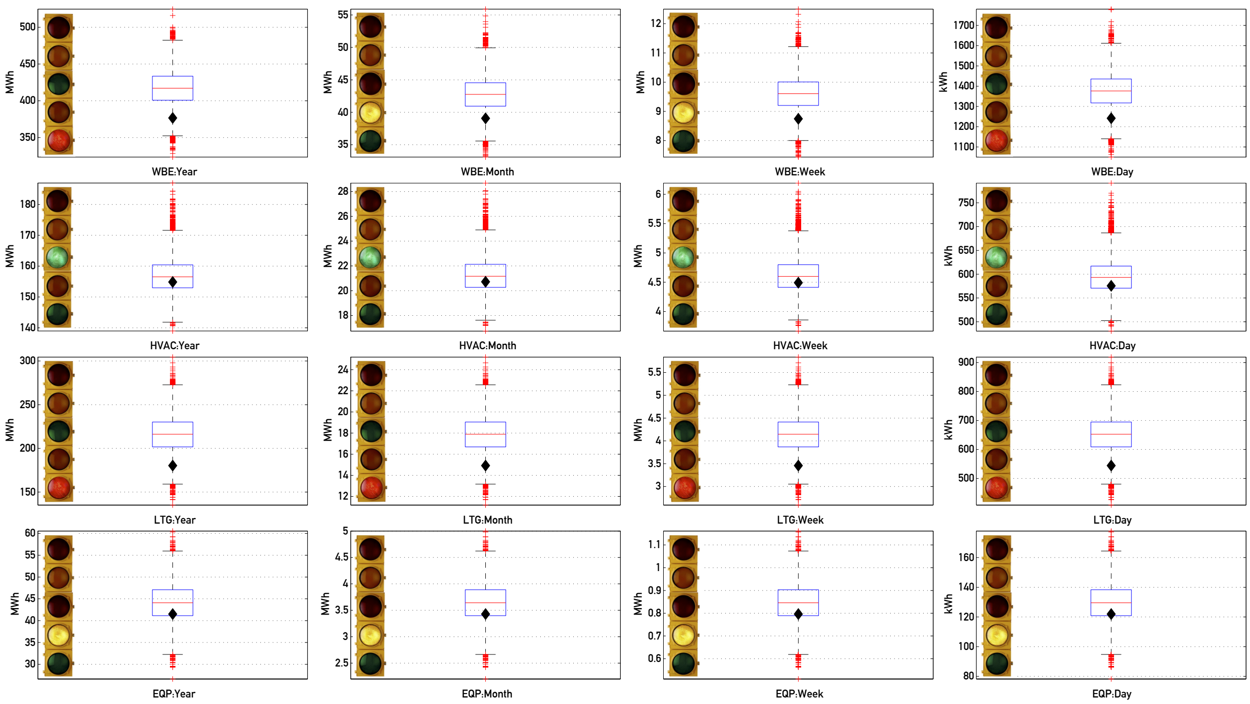

Figure 27. Fault-free low consumption case beginning August 30 (measured consumption data are indicated by diamonds in each figure)

4.1.2 Faulted Scenarios

In the faulted scenarios, the three cases are drawn from much wider distributions, as shown in Figure 23.

4.1.2.1 High Energy Consumption Case

The high consumption case for August 30 shows consistency between WBE, HVAC, and LTG. RH lights are shown for all time scales and the EQP consumption is close to model expectation. However, because the EQP contribution to the total is small, the WBE signal is not swayed to show a low green light.

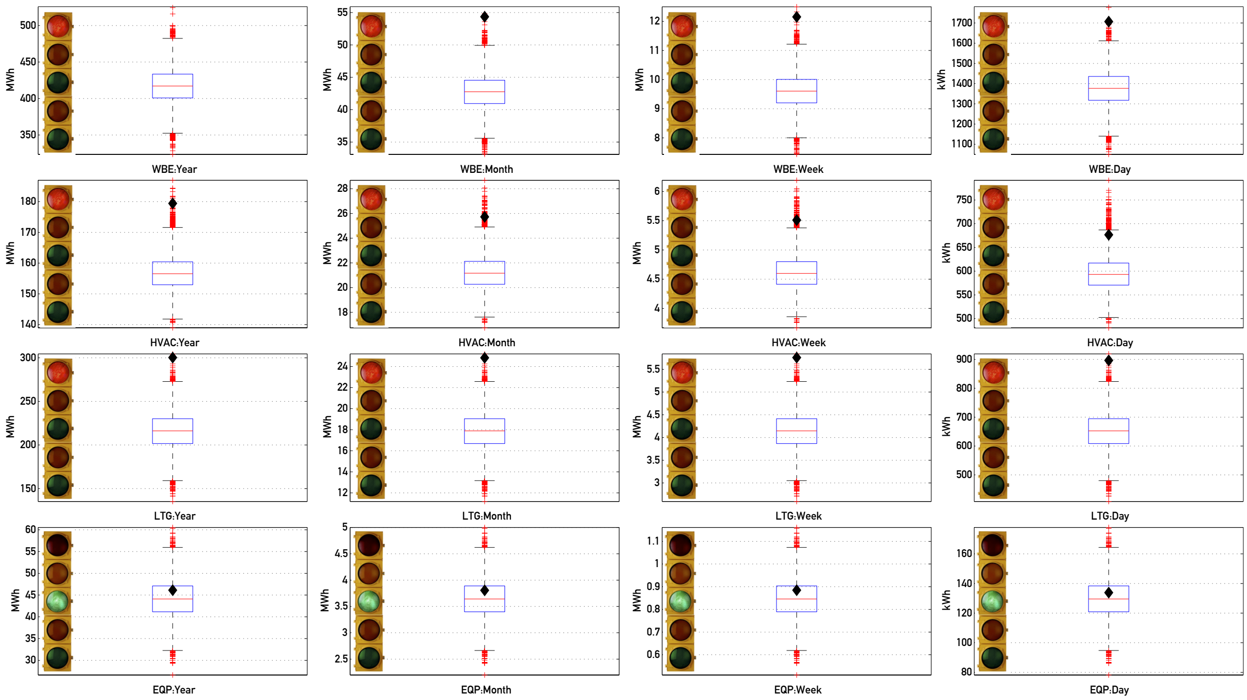

Figure 28. Faulted high consumption case beginning August 30 (measured consumption data are indicated by diamonds in each figure)

4.1.2.2 Medium Energy Consumption Case

On an annual basis, the medium consumption case leads to the expected green lights. On time scales of months and shorter, we can observe HVAC mild and strong underconsumption.

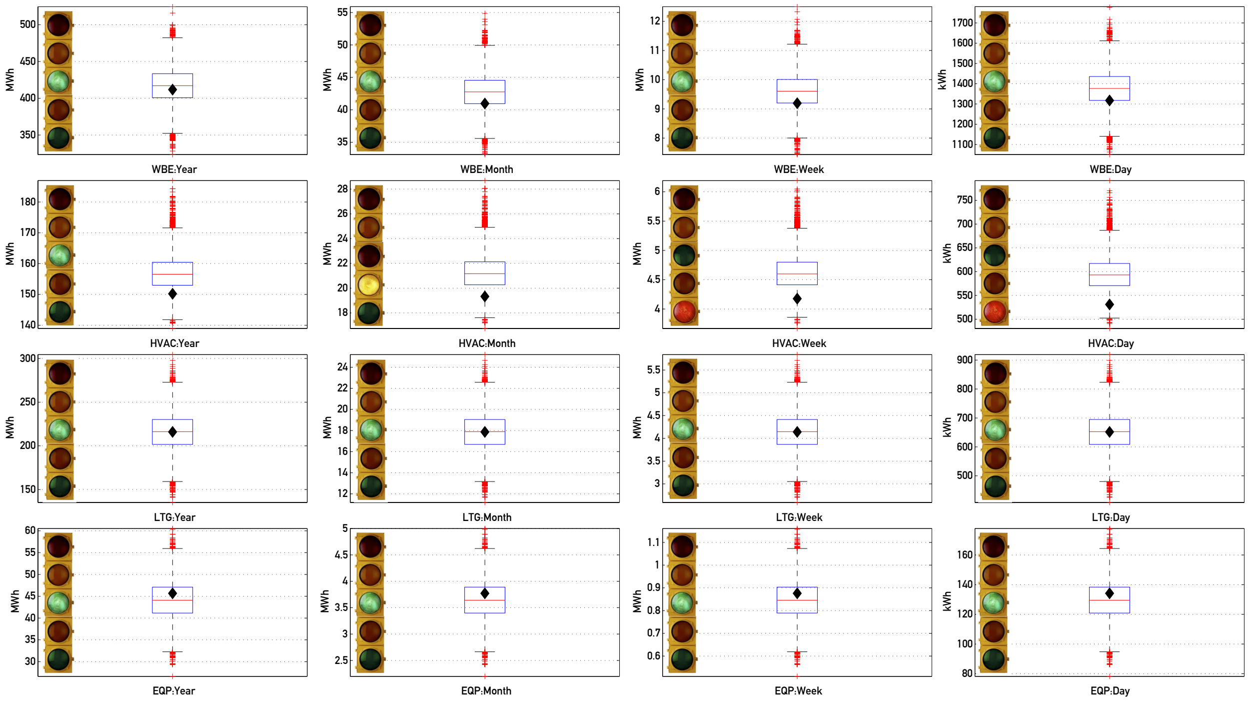

Figure 29. Faulted medium consumption case beginning August 30 (measured consumption data are indicated by diamonds in each figure)

4.1.2.3 Low Energy Consumption Case

The low consumption case at the 5th percentile of the faulted distribution shows a consistent RL light for all end uses and time scales, independent of season.

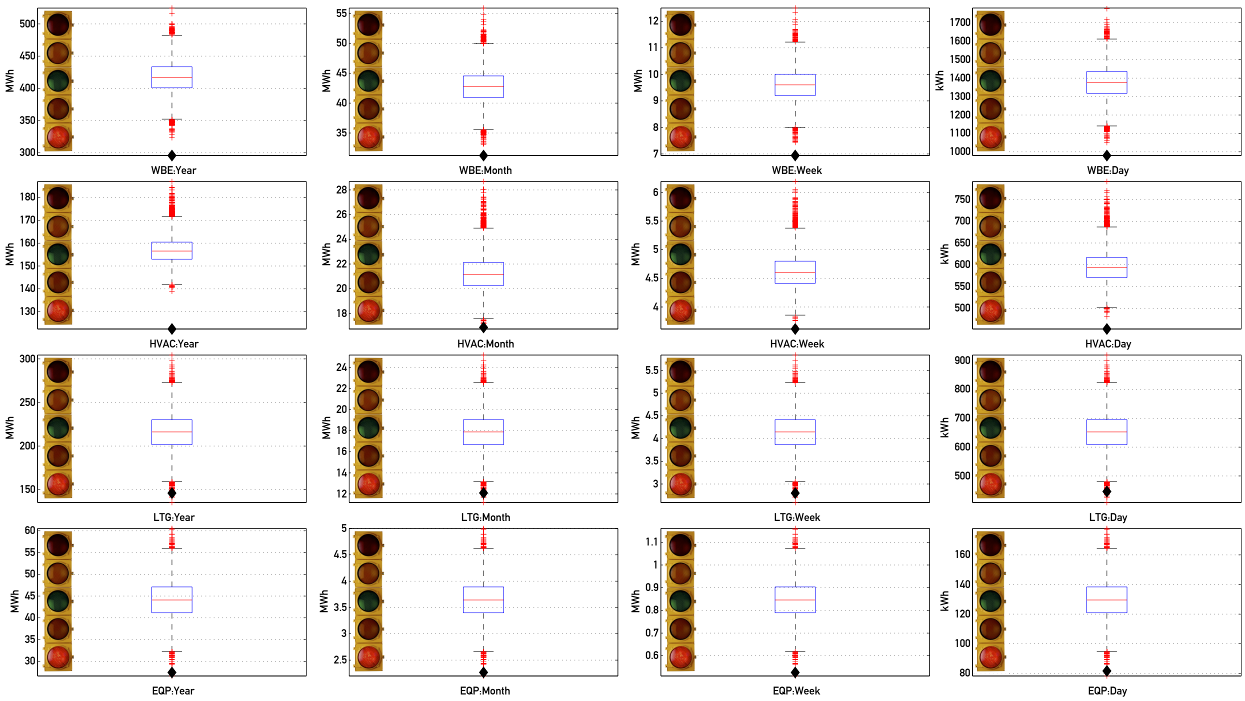

Figure 30. Faulted low consumption case beginning August 30 (measured consumption data are indicated by diamonds in each figure)

Finally, we present a sample illustration of how such a decision analysis tool would be deployed in the management of distributed commercial buildings. Imagine, a building operator is responsible for the energy-efficient operation of four buildings in a city. Building 1 appears to be healthy; all end uses show green signals for all four time scales; building 2 suffers from overconsumption problems in the HVAC system that manifest themselves in the last day, week, and month; building 3 exhibits underconsumption in LTG, especially during the last week, which could speak to failed light sources or delamping measures not yet accounted for in the model; finally, building 4 suffers from multiple symptoms: overconsumption in HVAC and EQP, and underconsumption in LTG.

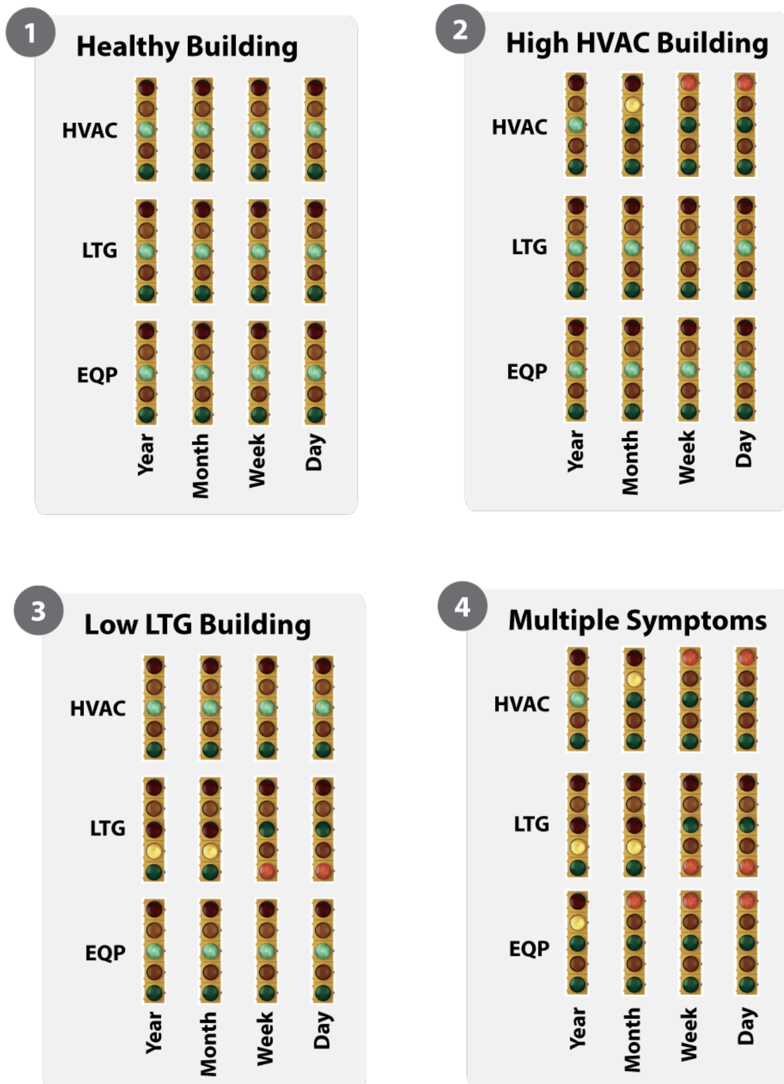

Figure 31. Example of four buildings managed by a building operator

4.2 Bayesian Parameter Updating Case Studies

Results related to the probabilistic inference and updating of the uncertain model parameters are presented for September 21, at which point measurements over the past 30 days are used to update the five input parameter distributions that are deemed uncertain. The high consumption case representing the 95th percentile of the fault-free conditional distributions is used to compute the likelihood functions for HVAC, LTG, and EQP for each of the nearly 10,000 parameter combinations. Based on the simplifying assumptions articulated above, we can then find the marginal posterior distribution for each selected uncertain parameter. Please note that white Gaussian noise with a signal-to-noise ratio of 25 was added to the time series data of the high consumption case to simulate common measurement noise affecting building measurements. Recent work by the same authors has shown the Bayesian inference approach to be robust with respect to a wide range of signal-to-noise ratios and noise colors (Pavlak et al., 2014).

Table 9 shows the nominal values used to generate the prior input parameter distributions as well as the parameter values associated with the low, medium, and high cases investigated in this section. The latter represent the ground truth values that will be compared to the posterior distributions for each model parameter to determine whether the measured data are used to update our belief of the uncertain parameters in a way that is consistent with the ground truth data.

The table shows that several individual parameters appear inconsistent with the case they belong to. As one example, in the low consumption case, the DX coil-rated COP is 3.1, which is below the nominal value. One would expect a higher COP to be associated with the low consumption case. However, given the tradeoffs between lighting and equipment power consumption and the efficiency of the cooling equipment, the low consumption case, at the 5th percentile of 10,000 simulation runs, was the result of a less efficient RTU with strongly reduced lighting and equipment power densities. The median consumption case resulted from a slightly higher lighting power density, lower equipment power density, lower occupant density, and higher RTU COP, all relative to the nominal values. The high consumption case, at the 95th percentile of all cases, is characterized by higher lighting, equipment, and occupancy densities, and lower HVAC equipment efficiency. In this case of higher consumption, the individual parameter values are all consistent with the theme of the case.

Later sections discuss that whatever tradeoffs were at play in leading to the low, medium, and high cases, the Bayesian parameter updating process is changing the posterior parameter distributions toward the ground truth values that form the basis of the measured (here surrogate) consumption data. To that effect, each of the following figures 32 to 46 shows the sampled prior distribution of the uncertain parameter as blue bars, the sampled posterior distribution as red bars, and the ground truth value that formed the basis of the surrogate measured data as a green vertical line.

Gas heating efficiency should have no impact on electricity consumption; thus, increased electricity consumption should be independent from gas heating coil efficiency. All the figures showing gas heating efficiency distributions illustrate that the gas heating efficiency posterior distribution is being smeared out; i.e., becoming less informative, because the evidence used in the likelihood function does not offer any clear clues about how to shape the posterior. Although we show the prior and posterior distributions for gas heating efficiency for all three cases, the independence of electricity consumption from gas heating efficiency is seen in a widening posterior in each case.

Table 9. Building Model Truth Parameters

Parameter	Nominal	Low	Medium	High	Units
Lighting power density	32.30	26.99	33.09	36.15	W/m^2
Equipment power density	5.23	4.92	4.96	5.94	W/m^2
Occupant density	0.141	0.149	0.137	0.151	per/m^2
DX coil rated COP	3.20	3.10	3.39	2.94	-
Gas heating coil efficiency	80	74	70	77	%

4.2.1 High Energy Consumption Case

Figures 32 through 36 clearly illustrate how the measured data would be harnessed to update our belief about the uncertain parameters. Each figure shows the empirical prior distribution as blue bars; the empirical posterior distribution is shown as red bars. Where the two distributions overlap, a darker, purple hue appears. As stated above, in the high energy consumption case, all individual building parameter truth values are consistent with the theme of high energy consumption. Lighting and equipment power density posteriors move to higher values relative to the nominal values that served as the mean of the normal prior distributions and gravitate toward the truth values (green vertical lines) used to generate the surrogate measured data. Similarly, occupancy densities in people per square meter are also slightly higher and the DX coil-rated COP is significantly lower than the nominal value, gravitating toward the truth values. Thus, the Bayesian inference "learns" the truth values that form the basis of the measured data.

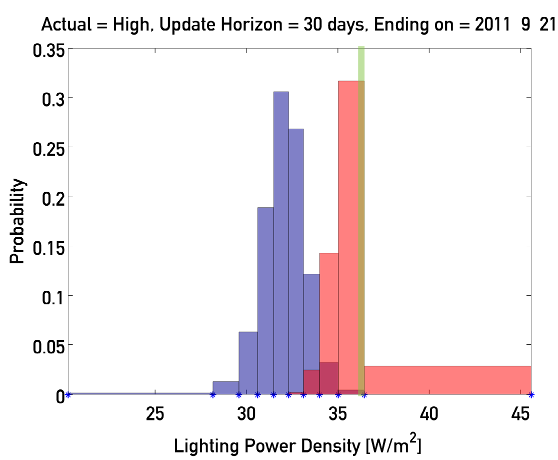

Figure 32. Lighting power density prior (blue) and posterior (red) distributions on September 21 based on past 30 days of high energy consumption. Truth value is shown as a green vertical line.

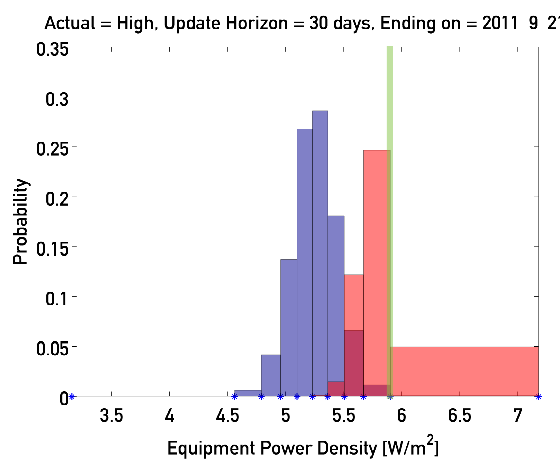

Figure 33. Equipment power density prior (blue) and posterior (red) distributions on September 21 based on past 30 days of high energy consumption. Truth value is shown as a green vertical line.

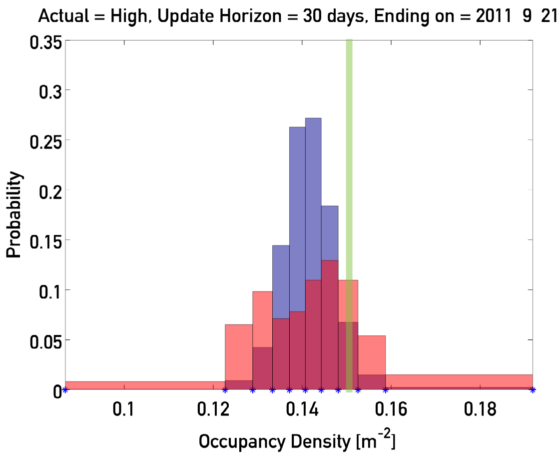

Figure 34. Occupant density prior (blue) and posterior (red) distributions on September 21 based on past 30 days of high energy consumption. Truth value is shown as a green vertical line.

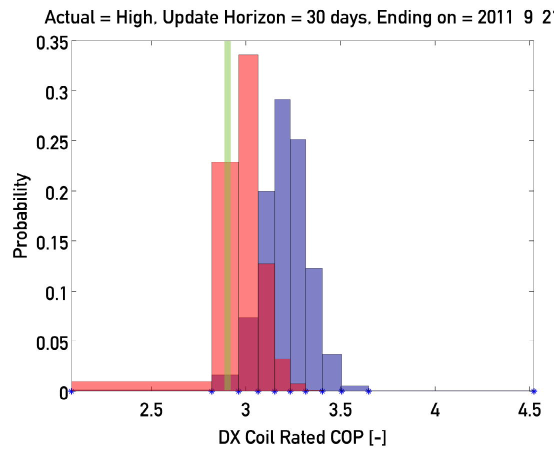

Figure 35. DX Coil Rated COP prior (blue) and posterior (red) distributions on September 21 based on past 30 days of high energy consumption. Truth value is shown as a green vertical line.

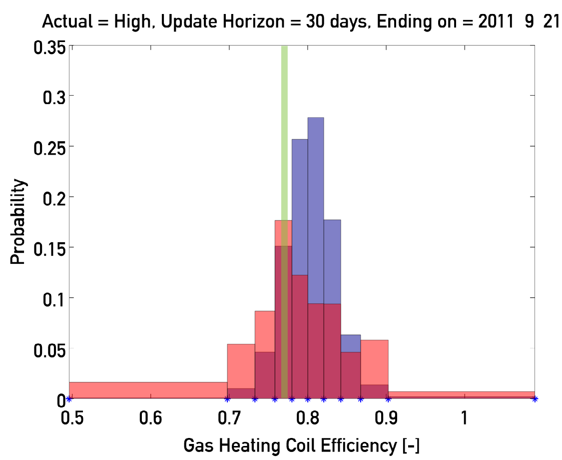

Figure 36. Gas heating coil efficiency prior (blue) and posterior (red) distributions on September 21 based on past 30 days of high energy consumption. Truth value is shown as a green vertical line.

4.2.2 Medium Energy Consumption Case

Figures 37 through 41 show how in the medium consumption case, the data reveal the tradeoffs that form the basis of the medium consumption case: A slightly higher lighting power density is compensated for by a significantly lower equipment power density, because these two have the identical effects of adding convective internal gains to the sensible energy balance, paired with slightly higher COPs. Occupant density distribution has not materially changed from prior to posterior in the medium consumption case. As in the high consumption case, the posterior distributions (except for gas heating efficiency, as explained above) have moved in the direction of the truth values that form the foundation of the surrogate measured data.

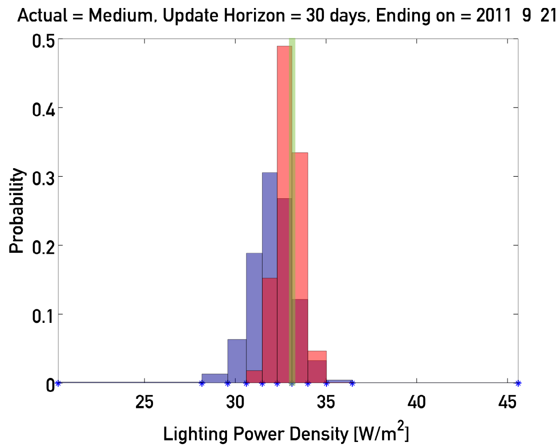

Figure 37. Lighting power density prior (blue) and posterior (red) distributions on September 21 based on past 30 days of medium energy consumption. Truth value is shown as a green vertical line.

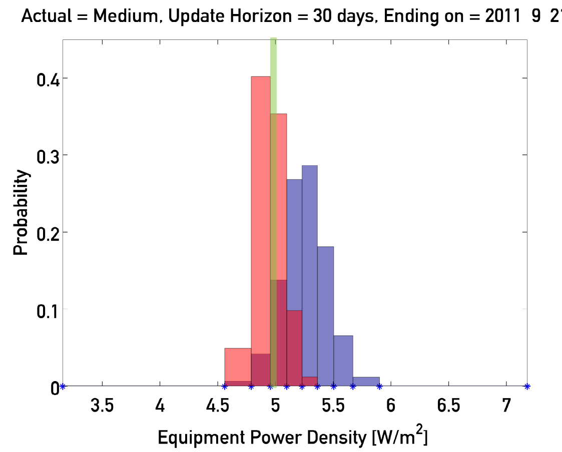

Figure 38. Equipment power density prior (blue) and posterior (red) distributions on September 21 based on past 30 days of medium energy consumption. Truth value is shown as a green vertical line.

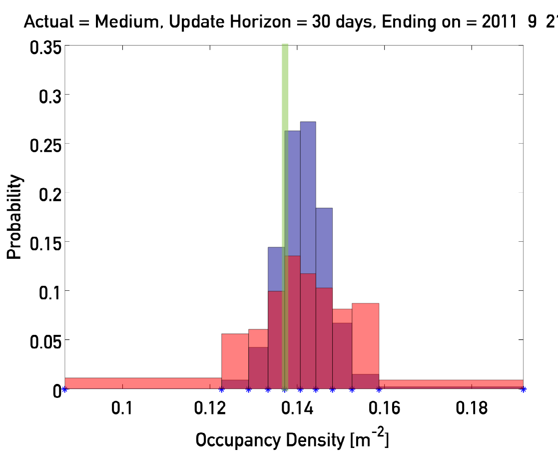

Figure 39. Occupant density prior (blue) and posterior (red) distributions on September 21 based on past 30 days of medium energy consumption. Truth value is shown as a green vertical line.

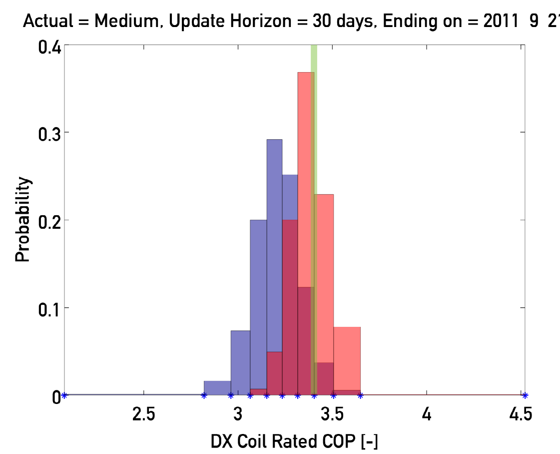

Figure 40. DX Coil Rated COP prior (blue) and posterior (red) distributions on September 21 based on past 30 days of medium energy consumption. Truth value is shown as a green vertical line.

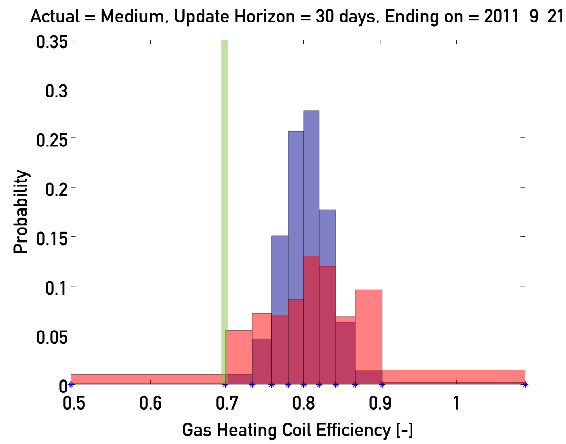

Figure 41. Gas heating coil efficiency prior (blue) and posterior (red) distributions on September 21 based on past 30 days of medium energy consumption. Truth value is shown as a green vertical line.

4.2.3 Low Energy Consumption Case

Figures 42 through 46 again clearly illustrate how the measured data would be harnessed to update our belief about the uncertain parameters. In the low consumption case, the data suggest significantly lower lighting and equipment power densities, although occupant density seems to materially impact the measured data, which lead to a virtually unchanged posterior.

As shown in Table 9, the truth value of the DX coil-rated COP is slightly lower than the nominal value, which is opposite to the theme of lower energy consumption. As explained above, the slightly inferior COP is more than compensated for by significantly lower lighting and equipment power densities. The posterior COP distribution is close[2] to the prior but slightly less than it, feels like something is missing here suggesting that the Bayesian inference has "learned" the truth value.

As before, electricity consumption should not and does not have informative power for gas heating efficiency, leaving the posterior smeared out relative to the prior.

---

[2] A very heuristic, visual interpretation of "close" was used. We simply encourage the reader to determine in which direction the posterior distribution mass has been moving: to the left, to the right, or virtually unchanged relative to the prior distribution. In particular, the point of using such loose language is to avoid comparing the empirical prior and posterior distributions with a more rigorous metric such as the maximum distance of the two cumulative distribution functions as used in the two-sample Kolmogorov-Smirnof test. Future work will look into more rigorous metrics to automate the update process. The point we wanted to make in this work, however, is that evidence is collected and used to inform updates of the input parameter distributions.

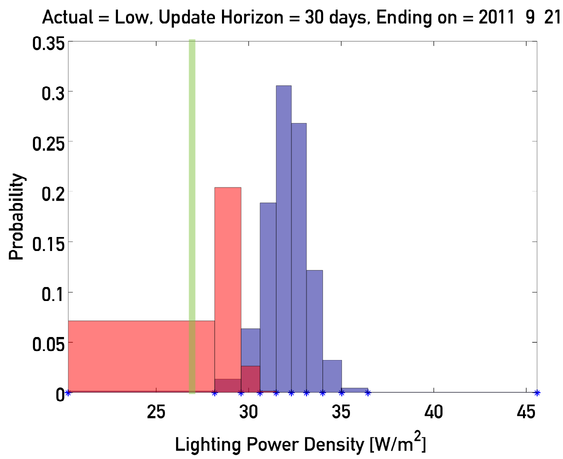

Figure 42. Lighting power density prior (blue) and posterior (red) distributions on September 21 based on past 30 days of low energy consumption. Truth value is shown as a green vertical line.

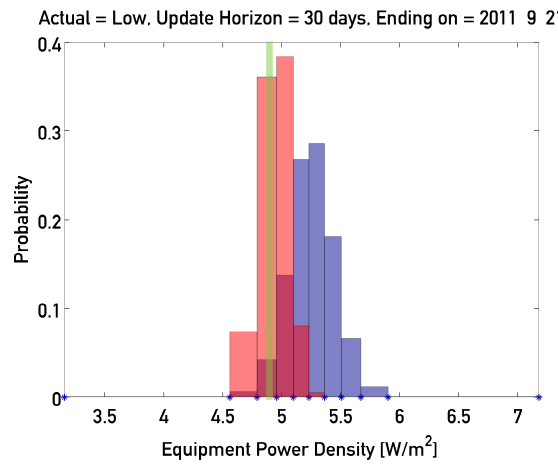

Figure 43. Equipment power density prior (blue) and posterior (red) distributions on September 21 based on past 30 days of low energy consumption. Truth value is shown as a green vertical line.

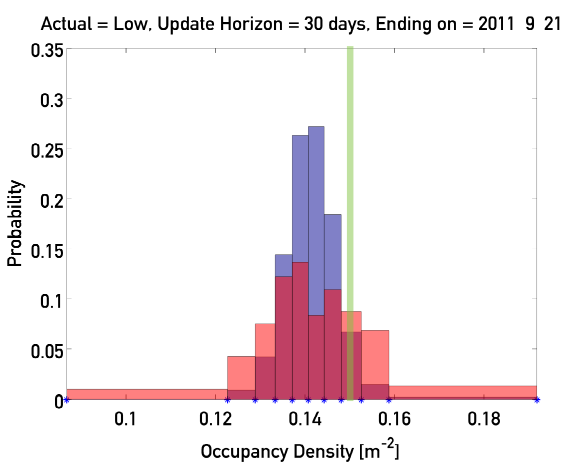

Figure 44. Occupant density prior (blue) and posterior (red) distributions on September 21 based on past 30 days of low energy consumption. Truth value is shown as a green vertical line.

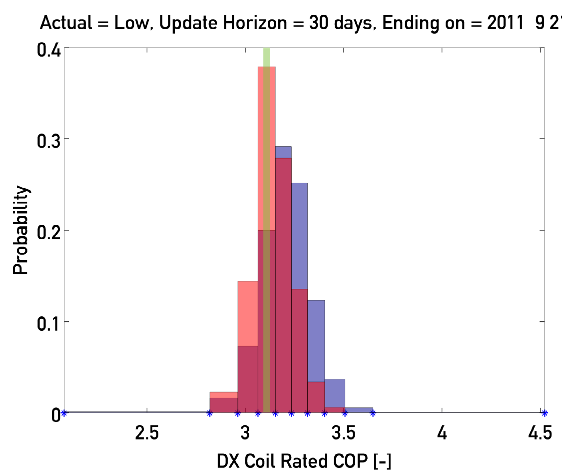

Figure 45. DX Coil Rated COP prior (blue) and posterior (red) distributions on September 21 based on past 30 days of low energy consumption. Truth value is shown as a green vertical line.

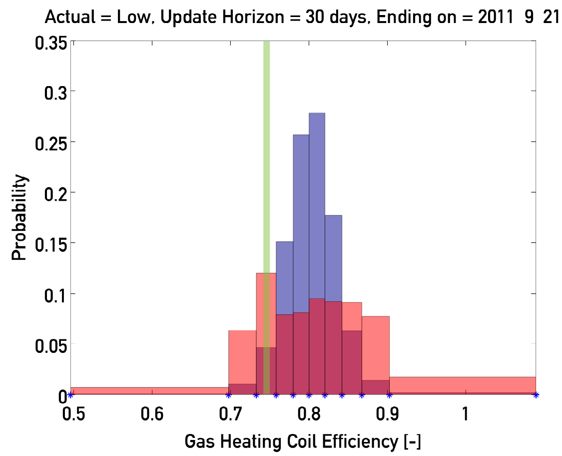

Figure 46. Gas heating coil efficiency prior (blue) and posterior (red) distributions on September 21 based on past 30 days of low energy consumption. Truth value is shown as a green vertical line.

5 Summary and Conclusions

A prototype energy signal tool was demonstrated for operational whole-building and system-level energy performance assessment. The purpose of the tool is to give an assessment that a building operator or other user can quickly comprehend. Toward this end, the energy signal tool estimates energy use for various end uses from a low-order lumped-parameter model, taking into account uncertainty (via a Monte Carlo method) in model parameters and inputs. The result of the modeling phase is a probability distribution over estimated energy use. The range of estimated energy use is divided into intervals based on the observed energy use, and the probability that energy use is in an interval is computed as the mass of the estimated energy use distribution in that interval. An indicator (traffic light color) is chosen to minimize misclassification cost. Model parameter distributions are adjusted over time via Bayesian updating.

The experimental study investigated whole-building energy signal accuracy in the presence of uncertainty and faults at the submetered level, which may lead to tradeoffs at the whole-building level that are not detectable without submetering. Submetering of end uses is recommended to avoid confounding underconsumption and overconsumption among various end uses. An example of four building energy signal displays is offered to illustrate energy performance features that could be detected by the energy signal tool. The Bayesian inference results presented show that observations can be used to periodically update model parameter distributions and that the posterior distributions indeed gravitate toward the ground truth parameter values that formed the basis of the surrogate measured data. We presented results for a 30-day learning cycle.

Future improvements in the inference process would eliminate the assumptions of temporal independence of subsequent observations of a particular variable and structural independence of multiple observed variables. Accounting for covariance among observed variables will help to better attribute observations to individual model parameters.

Bibliography

Attia, S.; Gratia, E.; Herde, A.D.; Hensen, J.L. (2012). "Simulation-based decision support tool for early stages of zero-energy building design." *Energy and Buildings* 49(0); pp. 2 – 15.

Augenbroe, G.; Castro, D.; Ramkrishnan, K. (2009). "Decision model for energy performance improvements in existing buildings." *Journal of Engineering, Design and Technology* 7(1); pp. 21 – 36.

Balcomb, J.; Curtner, A. (2000). "Multi-criteria decision-making process for buildings." *Energy Conversion Engineering Conference and Exhibit*, Vol. 1, pp. 528 – 535. Las Vegas, NV, USA: IEEE.

Basso, N.; Garavaglia, E.; Sgambi, L.; Imagawa, N. (2013). *Natural hazards vs. Decision-making processes in buildings life cycle management*. New York, NY, USA: CRC Press.

Bauermann, K.; Spiecker, S.; Weber, C. (3 2014). "Individual decisions and system development Integrating modelling approaches for the heating market." *Applied Energy* 116; pp. 149–158.

Booth, A.; Choudhary, R.; Spiegelhalter, D. (Feb. 2012). "Handling uncertainty in housing stock models." *Building and Environment* 48(0); pp. 35–47.

Bracken, C.; Rajagopalan, B.; Prairie, J. (Mar. 2010). "A multisite seasonal ensemble streamflow forecasting technique." *Water Resources Research* 46(3); pp. 1–12.
URL `http://doi.wiley.com/10.1029/2009WR007965`

Brandemuehl, M.; Shauna, G.; Inger, A. (1993). "HVAC2 Toolkit: Algorithms and Subroutines for Secondary HVAC System Energy Calculations." *ASHRAE, Atlanta, GA* .

Braun, J.E.; Chaturvedi, N. (2002). "An inverse gray-box model for transient building load prediction." *HVAC&R Research* 8(1); pp. 73–100.

Burkhart, M.C.; Heo, Y.; Zavala, V.M. (2014). "Measurement and verification of building systems under uncertain data: A Gaussian process modeling approach." *Energy and Buildings* 75; pp. 189 – 198.

Chaturvedi, N.; Braun, J.; Bernhard, R. (2000). *Analytical Tools for Dynamic Building Control: Implementation of Thermal Storage in Building Mass*. American Society of Heating, Refrigerating and Air-Conditioning Engineers.

Choi, J.H.; Aziz, A.; Loftness, V. (2009). "Decision support for improving occupant environmental satisfaction in office buildings: The relationship between sub-set of IEQ satisfaction and overall environmental satisfaction." *Ninth International Conference of Healthy Buildings*, p. #747. Syracuse, NY, USA.

Cipra, B.A. (2000). “The best of the 20th century: Editors name top 10 algorithms.” *SIAM news* 33(4); pp. 1–2.

Crawley, D.B.; Lawrie, L.K.; Winkelmann, F.C.; Buhl, W.F.; Huang, Y.J.; Pedersen, C.O.; Strand, R.K.; Liesen, R.J.; Fisher, D.E.; Witte, M.J.; et al. (2001). “EnergyPlus: creating a new-generation building energy simulation program.” *Energy and Buildings* 33(4); pp. 319–331.

Das, S.; Chew, M.; Poh, K.L. (2010). “Multi-criteria decision analysis in building maintainability using analytical hierarchy process.” *Construction Management and Economics* 28(10); pp. 1043 – 1056.

De Farias, C.; Soares, H.; Pirmez, L.; Delicato, F.; Santos, I.; Carmo, L.F.; De Souza, J.; Zomaya, A.; Dohler, M. (2014). “A control and decision system for smart buildings using wireless sensor and actuator networks.” *European Transactions on Telecommunications* 25(1); pp. 120 – 135.

De Wit, S.; Augenbroe, G. (2002). “Analysis of uncertainty in building design evaluations and its implications.” *Energy and Buildings* 34(9); pp. 951 – 958.

Deru, M.; Field, K.; Studer, D.; Benne, K.; Griffith, B.; Torcellini, P.; Halverson, M.; Winiarski, D.; Liu, B.; Rosenberg, M.; Huang, J.; Yazdanian, M.; Crawley, D. (2010). *U.S. Department of Energy Commercial Reference Building Models of the National Building Stock.* Washington, DC: U.S. Department of Energy, Energy Efficiency and Renewable Energy, Office of Building Technologies.

Diakaki, C.; Grigoroudis, E.; Kabelis, N.; Kolokotsa, D.; Kalaitzakis, K.; Stavrakakis, G. (2010). “A multi-objective decision model for the improvement of energy efficiency in buildings.” *Energy* 35(12); pp. 5483 – 5496.

Diakaki, C.; Grigoroudis, E.; Kolokotsa, D. (2013). “Performance study of a multi-objective mathematical programming modelling approach for energy decision-making in buildings.” *Energy* 59; pp. 534 – 542.

Dodier, R.; Kreider, J. (1999). “Whole Building Energy Diagnostics.” *ASHRAE Trans* 105(1); pp. 579–589.

Dodier, R.H.; Curtiss, P.S.; Kreider, J.F. (1998). “Small-scale on-line diagnostics for an HVAC system.” *Transactions-American Society Of Heating Refrigerating And Air Conditioning Engineers* 104; pp. 530–539.

DOE, U. (2010). “EnergyPlus Engineering Reference.” *The Reference to EnergyPlus Calculations* .
URL `http://apps1.eere.energy.gov/buildings/energyplus/pdfs/engineeringreference.pdf`

Filippoupolitis, A.; Gelenbe, E. (2009). "A decision support system for disaster management in buildings." *Summer Computer Simulation Conference*, pp. 141 – 147. Society for Modeling & Simulation International.

Florita, A.R.; Brackney, L.J.; Otanicar, T.P.; Robertson, J. (2013). "Classification of Commercial Building Electrical Demand Profiles for Energy Storage Applications." *Journal of Solar Energy Engineering* 135(3); p. 031,020.

Gulbinas, R.; Jain, R.K.; Taylor, J.E. (2014). "BizWatts: A modular socio-technical energy management system for empowering commercial building occupants to conserve energy." *Applied Energy* In-Press.

Gultekin, P.; Anumba, C.J.; Leicht, R.M. (2013). "Towards an integrated process model and decision support system for high performance green retrofits." *Architectural Engineering Conference 2013*, pp. 912 – 923. State College, PA, United states.

Heo, Y.; Augenbroe, G.; Choudhary, R. (2011). "Risk analysis of energy-efficiency projects based on bayesian calibration of building energy models." *Twelth Conference of International Building Performance Simulation Association*, pp. 2579 – 2586. Sydney, AUS.

Heo, Y.; Zavala, V.M. (2012). "Gaussian process modeling for measurement and verification of building energy savings." *Energy and Buildings* 53; pp. 7 – 18.

ISO, E. (2007). "13790: 2007." *Energy performance of buildings-Calculation of energy use for space heating and cooling* .

Jaynes, E.T. (2003). *Probability theory: the logic of science*. Cambridge university press.

Judkoff, R.; Balcomb, J.; Hancock, C.; Barker, G.; Subbarao, K. (2000). *Side-By-Side Thermal Tests of Modular Offices: A Validation Study of the STEM Method*. NREL Report TP-550-23940, National Renewable Energy Laboratory.

Judkoff, R.; Wortman, D.; O'Doherty, B.; Burch, J. (2008/1983). *Methodology for Validating Building Energy Analysis Simulations*. NREL Report No. TP-550-42059., National Renewable Energy Laboratory, Golden, CO.

Kiluk, S. (11 2014). "Dynamic classification system in large-scale supervision of energy efficiency in buildings." *Applied Energy* 132; pp. 1–14.

Kolokotsa, D.; Diakaki, C.; Grigoroudis, E.; Stavrakakis, G.; Kalaitzakis, K. (2009). "Decision support methodologies on the energy efficiency and energy management in buildings." *Advances in Building Energy Research* 3(1); pp. 121 – 146.

Lauret, P.; Miranville, F.; Boyer, H.; Garde, F.; Adelard, L. (May 2006). "Bayesian parameter estimation of convective heat transfer coefficients of a roof-mounted radiant barrier system." *Journal of Solar Energy Engineering* 128; pp. 213 – 225.

Lee, B.D.; Sun, Y.; Augenbroe, G.; Paredis, C.J. (2013a). "Towards better prediction of building performance: A workbench to analyze uncertainty in building simulation." *Thirteenth International Conference of the International Building Performance Simulation Association*, pp. 1231 – 1238. Chambery, France.

Lee, S.H.; Augenbroe, G.; Lee, J.K.; Zhao, F. (2013b). "A design methodology for energy infrastructures at the campus scale." *Computer-Aided Civil and Infrastructure Engineering* 28(10); pp. 753 – 768.

Lee, S.; Liu, Y.; Chunduri, S.; Solnosky, R.L.; Messner, J.I.; Leicht, R.M.; Anumba, C.J. (2012). "Development of a process model to support integrated design for energy efficient buildings." *International Conference on Computing in Civil Engineering*, pp. 261 – 268. Clearwater Beach, FL, USA.

Li, Z.; Heo, Y.; Augenbroe, G. (2009). "HVAC design informed by organizational simulation." *Eleventh International IBPSA Conference*, pp. 2198 – 2203. Glasgow, UK.

Mohseni, H.; Setunge, S.; Zhang, G.M.; Wakefield, R. (2013). "Condition monitoring and condition aggregation for optimised decision making in management of buildings." *Applied Mechanics and Materials* 438-439; pp. 1719 – 1725.

Moon, H.J.; Augenbroe, G. (2008). "Empowerment of decision-makers in mould remediation." *Building Research and Information* 36(5); pp. 486 – 498.

Neumann, C.; Jacob, D.; Burhenne, S.; Florita, A.; Burger, E.; Schmidt, F. (2011). *Model-Based Methods for Fault Detection and Optimization in Building Operations (Modellbasierte Methoden für die Fehlererkennung und Optimierung im Gebäudebetrieb).* Fraunhofer ISE.

Pavlak, G.; Florita, A.; Henze, G.; Rajagopalan, B. (2014). "Comparison of Traditional and Bayesian Calibration Techniques for Gray-Box Modeling." *Journal of Architectural Engineering* 20(2); p. 04013,011.

Piotr, R.; Laurence, B.; Alison, C.; Ahmed, A.S. (2012). "Decision making aid for selection of renewable/sustainable energy systems for buildings." *International Conference on Sustainable Design and Construction*, pp. 306 – 313. Kansas City, MO, USA: ASCE.

Rafiq, M. (2000). "Importance of Pareto optimum solutions in making informed decisions in engineering design." *Eighth International Conference on Computing in Civil and Building Engineering*, Vol. 2, pp. 1325 – 1333. Stanford, CA, USA: ASCE.

Sanctis, G.D.; Fischer, K.; Kohler, J.; Fontana, M.; Faber, M. (2011). *A probabilistic framework for generic fire risk assessment and risk-based decision making in buildings*. Zurich, Switzerland: CRC Press.

Seem, J. (1987). *Modeling of heat transfer in buildings*. Ph.D. Thesis, University of Wisconsin-Madison.

Sivia, D.; Skilling, J. (2006). “Parameter estimation II.” *Data Analysis: A Bayesian Tutorial*, Chap. 3, pp. 35 – 77. Oxford University Press.

Subbarao, K. (1988a). *PSTAR - Primary and Secondary Terms-Analysis and Renormalization: A Unified Approach to Building and Energy Simulations and Short-Term Testing; A Summary*. NREL Report TR-254-3347, National Renewable Energy Laboratory.

——— (1988b). *PSTAR - Primary and Secondary Terms Analysis and Renormalization: A Unified Approach to Building Energy Simulations and Short-Term Monitoring*. NREL Report TR-254-3175, National Renewable Energy Laboratory.

Subbarao, K.; Burch, J.; Hancock, C.; Lekov, A.; Balcomb, J. (1988). *Short-term Energy Monitoring (STEM): Application of the PSTAR Method to a Residence in Fredericksburg, Virginia.* NREL Report TR-254-3356, National Renewable Energy Laboratory.

Subbarao, K.; Mort, D.; Burch, J. (1985). *Short-Term Measurements for the Determination of Envelope Retrofit Performance*. NREL Report TP-253-2639, National Renewable Energy Laboratory.

Sun, Y.; Heo, Y.; Tan, M.; Xie, H.; Jeff Wu, C.; Augenbroe, G. (2014). “Uncertainty quantification of microclimate variables in building energy models.” *Journal of Building Performance Simulation* 7(1); pp. 17 – 32.

Takizawa, A.; Kawamura, H.; Tani, A. (2000). “Simulation of urban system “as it could be” by multiagent model.” *Eighth International Conference on Computing in Civil and Building Engineering*, Vol. 2, pp. 1566 – 1573. Stanford, CA, USA: ASCE.

Thompson, B.P.; Bank, L.C. (2010). “Use of system dynamics as a decision-making tool in building design and operation.” *Building and Environment* 45(4); pp. 1006 – 1015.

Ugwu, O.; Anumba, C.; Newnham, L.; Thorpe, A. (2000). “Agent-oriented collaborative design of industrial buildings.” *Eighth International Conference on Computing in Civil and Building Engineering*, Vol. 1, pp. 333 – 340. Stanford, CA, USA: ASCE.

Vinh, A. (2009). “Computer-based monitoring for decision support systems and disaster preparedness in buildings.” *Systemics, Cybernetrics and Informatics* 7; pp. 51–56.

Wang, L.; Greenberg, S.; Fiegel, J.; Rubalcava, A.; Earni, S.; Pang, X.; Yin, R.; Woodworth, S.; Hernandez-Maldonado, J. (2 2013). “Monitoring-based HVAC commissioning of an existing office building for energy efficiency.” *Applied Energy* 102; pp. 1382–1390.

Zeiler, W.; Maaijen, R.; Maassen, W. (2012). “Decision support for sustainable, healthier and more productive buildings.” *Tenth International Conference Healthy Buildings*, pp. 1–6. Brisbane, AUS.

Zhao, P.; Suryanarayanan, S.; Simoes, M.G. (2010). “An energy management system for building structures using a multi-agent decision-making control methodology.” *Industry Applications Society Annual Meeting*, pp. 1–8. Houston, TX, USA: IEEE.

Zhao, Y.; Wang, S.; Xiao, F. (12 2013). “Pattern recognition-based chillers fault detection method using Support Vector Data Description.” *Applied Energy* 112; pp. 1041–1048.